Distribution
Category UC-71

SAND84-2271
TTC-0532
Unlimited Release
Printed June 1985

SAND--84-2271

DE85 015088

TRANSPORTATION SYSTEM IMPACT LIMITER DESIGN USING RIGID POLYURETHANE FOAM

BY

G. W. Wellman
Sandia National Laboratories
Albuquerque, NM 87185

ABSTRACT

Techniques used to apply the finite element method to the analysis of rigid polyurethane foam that is confined by a thin, ductile metallic skin were investigated. The initial investigation covered the analysis of a simple geometry and loading condition of constrained and unconstrained foam using the constitutive relationships implied in the "Elastic-Plastic" and "Crushable Foam" material models in HONDO II and DYNA2D/3D. The final investigation consisted of the analysis of a series of tests of scale model impact limiters and comparison of the experimental and analytical results.

DISCLAIMER

CONTENTS

FIGURES

TABLES

1. INTRODUCTION

The structural design of transportation packaging is usually controlled by the regulatory hypothetical accident conditions. Of these conditions, the 30 foot drop onto an unyielding target is important to design of impact limiters. In the 30-foot drop event, the impact limiters undergo dynamic, large strain, nonlinear behavior over a short time duration. This type of analysis is quite complex. In addition to the complexity of the analysis itself, the behavior of rigid polyurethane foam enclosed by a thin metallic skin is not well known. Because of the analytical complexity and unknown material behavior, it is necessary to qualify the analysis procedures prior to the analysis of the transportation system for licensing.

This paper addressed the analytical concerns of using skinned rigid polyurethane foam impact limiters in two parts. First, the rigid foam behavior was investigated. A simple geometry (a short cylinder under uniform compression) was used to determine the analytical response of the finite element method code. A series of analyses using different material models (constitutive equations) with the outside radius of the cylinder constrained and unconstrained was performed. It was shown that the unconstrained "Elastic-Plastic" and the constrained "Crushable Foam" models provide an adequate representation of the rigid polyurethane foam. Second, the results of the investigation into foam analytical behavior were applied to the 30 foot drop event. A series of half-scale tests was performed. The analytical results were compared to the experimental results for these drop tests. The final impact limiter crush and the cask body accelerations were the primary parameters used for this comparison. These parameters were easily determined experimentally and were also important in addressing the safety of the package. The results of these comparisons showed that the analytical procedures used adequately represent the behavior of the impact limiters during the 30-foot drop. Because the same procedures are used in the analysis of full-scale impact limiters, these results may be used to qualify the analyses performed for the Beneficial Uses Shipping System (BUSS) cask safety analysis report[1].

2. RIGID POLYURETHANE FOAM DESCRIPTION

Rigid polyurethane foam displays mechanical properties that make it well suited for use in systems designed to absorb the energy from impact events such as the regulatory, 10 CFR71, 30-foot drop onto an unyielding target. As shown in a typical compression test result in Figure 1, this foam has an initial elastic region, followed by a very large flat plateau region, finally terminating in a region where the stress rises rapidly with small increments of strain (foam lock up). The low strain behavior is analogous to that seen in steel or other metallic alloys. In foam testing, however, 10 percent strain is typically used to determine the compressive strength, rather than the 0.2 percent offset used for yield strength of metals. The relatively flat plateau region can be defined as beginning at the 10 percent strain and extending to the 50 to 70 percent strain range (50 percent strain is generally chosen for conservatism and convenience). The increase in stress from the beginning to the end of the plateau region is approximately 50 percent of the compressive strength. This means that the average plastic modulus in the plateau region is approximately an order of magnitude less than the modulus in the initial elastic region. It is in this region, where large strains occur at relatively constant stress, that most of the strain energy from an impact event is absorbed. Following the plateau region (in the 70 to 90 percent strain range), foam"lock-up" occurs. This phenomenon is characterized by large increases in stress for small increases in strain. The tangent modulus in the "locked-up" region is several times higher than the initial elastic modulus. Because high stresses develop in this region, the impact energy attenuation properties of the foam are no longer favorable. Thus impact absorption systems should be designed such that foam strains do not exceed 50 percent. If this design condition can be achieved, then "lock-up" behavior at strains greater than 70 percent can be disregarded.

In addition to the desirable mechanical properties discussed above, rigid polyurethane foam also exhibits resistance to most chemicals and solvents, resistance to water absorption, and good dimensional stability to temperatures up to at least 250°F. Polyurethane foam will decompose when exposed to fire. However, in the hypothetical accident condition test series, the fire test occurs after the impact test and, thus, foam charring or decomposition will have no effect on package integrity. In conclusion, rigid polyurethane foam exhibits a number of highly desirable properties that make it an excellent choice for an energy absorbing material in transportation system impact limiter designs.

3. MATERIAL CHARACTERIZATION WITHIN THE FINITE ELEMENT METHOD

There are two material models in the HONDO II and DYNA2D/3D finite element analysis codes[2-4] that are appropriate for describing the behavior of rigid polyurethane foams. These two are the "Elastic-Plastic" and the "Soil and Crushable Foam" models.

The "Elastic-Plastic" model was designed to characterize ductile metals. The details of this model are shown in Figure 2. The input parameters, some of which are described in Figure 2, are Young's modulus (E), Poisson's Ratio (υ), yield stress (σ_0), hardening tangent modulus (E_t), and the hardening parameter (β). β, which defines the combination of isotropic (β=1) and kinematic (β=0) hardening to be used, is unimportant in this analysis of foam impact limiters because reverse yielding does not occur. E, σ_0, and E_t are defined for the rigid polyurethane foam as shown in Figure 3. Note, with the strain limited to about 50 percent, a straight line provides an adequate representation of the foam hardening. υ is defined using Young's modulus(E), the shear modulus (G), and the relationship $E = 2(1+\upsilon)G$.

The "Crushable Foam" model was designed to characterize foams, solids, and other void containing materials which compact under pressure. These materials exhibit pressure dependent behavior as shown in Figure 4. The input parameters are the shear modulus (G), the bulk unloading modulus (K_o), three yield function constants (a_0, a_1, a_2), the pressure cutoff for tensile fracture (F_p), and the pressure (P) versus logarithmic volumetric strain (-ln V) curve. The yield function (ϕ) is defined in terms of the second invariant of the stress (J_2), the pressure (P), and the three constants a_0, a_1, a_2 as follows:

$$\phi = J_2 - [a_0 + a_1 P + a_2 P^2] \ .$$

This permits a yield surface that varies quadratically with pressure. In this report, a simple cylindrical yield surface was chosen by a setting $a_1 = a_2 = 0$ and $a_0 = \sigma_0^2/3$ where σ_0 is the compressive strength of the foam in a uniaxial compression test. Because uniaxial compression test data is normally available, manipulation of this data is required to determine the input parameters to the "Crushable Foam" model. For rigid polyurethane foam, an estimate of G is available from the foam density relations. K_o and the P versus (-ln V) curve are derived from the uniaxial compression test stress-strain curve. The engineering strains from the compression test are converted to logarithmic strains. The engineering stresses are divided by three. These values are an estimate of the P versus (-ln V) curve. The initial elastic slope of the compression test modified similarly (one third the engineering stress divided by the logarithmic strain) provides an estimate of K_o. F_p is assigned a small magnitude but it is not operative during the impact limiter analysis. A more rigorous mathematical exposition of both the "Elastic-Plastic" and "Crushable Foam" material models is provided in References 2-4.

4. Material Characterization Verification

In order to determine the behavior of the "Elastic-Plastic" and "Crushable Foam" material models, a series of simple analyses was performed. A cylinder, ten inches in diameter by ten inches in height, was selected for the analysis investigation. The finite element analysis code "DYNA2D" was used to perform this nonlinear axisymmetric analysis. The cylinder was loaded in displacement control to a displacement consistent with an overall strain of 50 percent. Initially, four cases were analyzed. The cylinder was analyzed first with the outside radius free to expand and then with the outside radius constrained to prevent lateral expansion. Both material models were used. The results of primary interest in these analyses were the engineering stress-strain curves which were easily derived from the overall load-displacement curves. The comparison between the experimental stress-strain curve used as input to the material model and the analytical stress-strain curve derived from the finite element analysis can be used to determine the material model performance.

The approximation to the stress-strain curve used for input to the "Elastic-Plastic" material model for 1000 psi compressive strength foam is shown in Figure 5. The material model input parameter values are listed in Table I. The analysis results for the cylinder that was free to expand laterally are shown in Figure 6. The input curve (Fig. 5) and the analysis results curve (Fig. 6) are nearly identical. The very slight elevation of stress in the results curve is probably due to dynamic overshoot because the displacements were imposed over a relatively short time duration. In Figure 7 the analytical results for the cylinder that was constrained to prevent lateral expansion are shown. The input stress-strain curve again is the curve shown in Figure 5. The lateral constraint has a significant effect on the analytical stress-strain curve. The effective initial modulus is slightly greater than the elastic modulus input to the material model. The effective tangent modulus, in the strain-hardening portion of the curve, is more than five times the tangent modulus input to the material model.

The input parameters to the "Crushable Foam" material model are listed in Table II. Note that most of these parameters were extrapolated from uniaxial compression test results. These input parameters convert to the uniaxial stress-strain curve shown in Figure 8. The results from the analysis of the unconstrained cylinder using the "Crushable Foam" material are shown in Figure 9. Note that this analysis displays more instability (dyamic overshoot or vibration) in the initial elastic region than was present using the "Elastic Plastic" material model. The analysis shows no strain hardening behavior. The displacement pattern is also unusual as shown in Figure 10. The central bulge is unique to the analysis using this material model. While keystoning in the elements may serve to enhance this displacement pattern, the bulge was present in all analyses regardless of the zero energy mode suppression scheme used. Thus, it is regarded as a real displacement pattern. The analysis results for the constrained cylinder using the "Crushable Foam" material model are shown in Figure 11. There is some instability apparent in the initial elastic region, but much less than for the unconstrained cylinder analysis. The strain-hardening portion of the curve matches the uniaxial stress-strain input curve. The pressure-volumetric strain curve was represented using three straight line segments. Therefore, only a three straight line segment stress-strain curve is possible for output. A more accurate and detailed material description up to nine line segments can be input to the material model if necessary.

Based on the analytical stress-strain curves (Figures 6, 7, 9, 11), the following recommendations for analyzing rigid polyurethane foam are made. If the outside constraint (metallic skin, etc) is included in the analysis, the "Crushable Foam" model should be used. The "Elastic-Plastic" material model is not applicable in this case because the incompressibility assumption in plasticity theory causes behavior that is much too stiff. The more usual case for rigid foam impact limiters is for the metallic skin to be too thin to permit adequate modeling of the skin with the solid elements available in HONDOII or DYNA2D/3D. In this case, when the external constraint is not modeled, the "Elastic-Plastic" material model provides a better match with the experimental data than does the "Crushable Foam" model.

5. Impact Limiter Analysis

Rigid polyurethane foam contained by a thin (0.135 in. thick) 304 stainless steel skin was selected as the impact limiting system for the BUSS cask. The basic geometry of the one-half scale cask and impact limiter test model is shown in Figure 12. Because it is impossible to efficiently model a thin skin using the "DYNA" series finite element analysis codes, the skin was neglected and the rigid foam modeled using the "Elastic-Plastic" material model. Preliminary design calculations led to selection of a foam density consistent with a 900 psi compressive yield strength (approximately 18 pounds per cubic foot). The foam in the impact limiters as actually manufactured was of approximately 1000 psi yield strength. At this density, the foam is essentially isotropic with negligible variation in properties between the parallel and perpendicular-to-bubble-rise orientations.

The three classical orientations for the 30-foot drop onto an unyielding target (end, side, and center of gravity over corner) were analyzed. HONDO II was used for the end drop and DYNA 3D for the side and center of gravity over corner drops. Because most of the deformation occurs within the impact limiter, the cask body was modeled using a coarse mesh while the impact limiter model employed a finer mesh. The impact limiters were attached analytically to the cask body using the "Tied Interface" option. Initial test results showed that the inner skin effectively prevented relative motion between the impact limiter inside diameter and the cask body outside diameter. Therefore, the tied interface attachment scheme is more consistent with the actual structural behavior than is a sliding interface. Cask body accelerations and impact limiter crush values were used for the primary comparison with experimental results.

The finite element mesh for the initial design one-half scale cask and impact limiters in the corner drop orientation is shown in Figure 13. Only one-half the structure is modeled due to the presence of a plane of symmetry. The explicit integration finite element code, DYNA3D, was used in the analysis. This corner drop was performed at 45° to vertical to correspond to the field test. This was a slightly greater angle than center of gravity over

corner orientation which was 38°from vertical. The impact limiter crush from the finite element analysis is shown in Figure 14. The final crush value, after elastic recovery, is approximately 3.2 in. The physical measurements of the actual impact limiter after the drop test yielded the same, 3.2 in., final crush value. The deformed shape at maximum crush (0.013 s. after impact) is shown in Figure 15. The experimental acceleration values from accelerometers mounted on the cask body are compared to the analytical accelerations in Figures 16 and 17. Accelerations in Figure 16 are parallel to the cask axis. Accelerations in Figure 17 are perpendicular to the cask axis at 45° to the fall direction. The analytical accelerations are from values extracted from the analysis every 0.001 s. The experimental values have been filtered at 1000 Hz. The agreement between the experimental and analytical results is good, both in the shape of the curves and in the peak magnitudes.

Other considerations led to a redesign of the impact limiters. The major change with a structural analysis significance was the removal of a 20-inch diameter cylindrical section of foam, located along the impact limiter axis as shown in Figure 18. This half-scale, new design impact limiter and cask was analyzed in the side drop orientation. The mesh used is shown in Figure 19. Only one-fourth of the structure was modeled due to the two axes of symmetry. Again, DYNA 3D was used to perform the analysis. Figure 20 shows the impact limiter crush values as a function of time after impact. The final crush value, after elastic recovery, is approximately 2.1 in. The experimental crush value estimated from post-test impact limiter measurements is 2.0 in. The deformed shape at maximum impact limiter crush (0.008 s. after impact) is shown in Figure 21. The analytical accelerations on the cask body in the direction of fall are compared to the experimental accelerations in Figure 22. As in the corner drop, the analytical accelerations were extracted every 0.001 s. and the experimental accelerations were filtered at 1000 Hz. The analysis predicts the maximum acceleration rather well. However, the shapes of the acceleration-time curves do not match well, and the analysis predicts the maximum acceleration to occur about 0.006 s. later than was determined in the experiment.

The analytical and experimental investigations led to the understanding that the impact limiters were stiffer than optimum. Given the geometric constraints of the impact limiter design, a softer foam would result in lower cask body accelerations while not exceeding the maximum impact limiter crush values. The side drop is the critical orientation for optimizing the impact limiter. The cask must be stopped prior to contacting the unyielding surface with the lifting trunion. This establishes the limit on permissible impact limiter crush. A series of analyses led to the selection of a polyurethane foam with a 300 psi compressive strength in the transverse (perpendicular to rise) direction. This strength foam was consistent with the criteria of minimizing the cask body accelerations while preventing contact of the lifting trunions with the unyielding target.

Because of time constraints, it was decided to test the half- scale impact limiters with the minimum number of changes. Two of the old design (no axial hole) impact limiters were available. The original 900 psi foam was removed and the impact limiters were refoamed. The new foam strength, as installed, was 360 psi in the transverse direction (perpendicular-to-bubble-rise). This strength level was determined from samples removed from the actual impact limiters after foaming. This was a higher strength foam than desired, but it was deemed to be acceptable for the half-scale test.

The half-scale test of the lower strength foam was also conducted in the side drop orientation for several reasons. The side drop had been identified as the orientation that controlled the minimum foam strength (cask motion had to be stopped before the lifting trunions contacted the target). The impact limiter attachment scheme was most severely tested in a side drop. The effect of the axial hole in the impact limiter was minimized in the side drop orientation. Finally, the side drop was the easiest orientation in which to rig the half-scale cask for lifting prior to the drop.

The side drop analysis was again performed using DYNA3D. Because of the larger deflections encountered with the lower strength foam, a finer mesh with more regularly sized elements was produced for this analysis. As in the prior analysis, symmetry conditions permit the modeling of one fourth of the

structure as shown in Figure 23. As in all preceding impact limiter analyses, the "Elastic-Plastic" material model was used. The material properties input to the model were consistent with 360 psi compressive strength foam tested perpendicular to bubble rise.

At the 300 psi compressive strength perpendicular-to-rise, rigid polyurethane foam exhibits a lower (approximately 25% reduction) strength perpendicular-to-rise than parallel-to-rise. This anisotrophy was not included in the analysis because anisotropic material models are not currently available in DYNA3D. The stresses perpendicular to the principal crush direction were found to be small (due to the small Poisson's ratio in foam) and, therefore, ignoring the anisotropic behavior of the foam causes negligible error in the analysis.

As shown in Figure 24, the maximum value of impact limiter crush is approximately 4.4 in. at 0.014 s. after initial contact. This maximum crush value is followed by an elastic recovery to approximately 3.8 in. at 0.022 s. The actual final impact limiter crush value was estimated to be about 4 in. using post-test measurements. The deformed shape at maximum impact limiter crush is shown in Figure 25. The analytical and experimental comparison of the cask body accelerations in the direction of fall is shown in Figure 26. The experimental acceleration data was filtered at 1000 Hz and the analytical accelerations were extracted every 0.001 s. As in the previous side drop, the analytical and experimental peak accelerations were almost identical. However, the analytical acceleration peak was predicted to occur about 0.007 s. after the experimental peak. The reason the analytical acceleration peak occurs later in the side drop impact event than experimental peak has not been determined.

6. CONCLUSIONS

The results of an analytical and experimental investigation of rigid polyurethane foam contained in a thin metallic skin produced the following conclusions:

1. It is appropriate to use the constitutive relationships in the "Crushable Foam" material model only if the external restraint (skin) is included in the analysis.

2. The constitutive relationships in the "Elastic-Plastic" material model adequately represent the behavior of rigid foam enclosed by a thin metallic skin when the skin is not included in the analysis. The mechanical properties of the foam are used as material model input and the skin is ignored.

3. For the complex geometry and loading of an impact limiter, minor modification of Conclusion 2 is required. The use of the "Elastic-Plastic" material model permits the exclusion of the skin on the impact limiter outer surface from the analysis. Because of the geometry, the impact limiter inner skin which is in close proximity to the cask wall cannot be totally ignored. This skin acts to prevent local foam deformation around the cask body. This behavior can be adequately represented using a "tied interface" connection between the cask and impact limiter.

4. Comparison of scale model drop tests with analyses shows that the analysis procedures outlined in this report adequately represent the actual drop event. Two parameters of primary importance in transportation cask design, impact limiter displacement, and cask body acceleration, were used in this comparison. Given the agreement of these parameters between analysis and test, it is assumed that the analysis procedure is adequately qualified to produce accurate results for similar systems. Application of these procedures to the full-scale BUSS cask and impact limiters is straightforward.

7. REFERENCES

1. "Beneficial Uses Shipping System (BUSS) Cask Safety Analysis Report for Packaging (SARP)," SAND83-0698 (Albuquerque, New Mexico: Sandia National Laboratories 1985).

2. Key, S. W.; Beisinger, Z. E.; Krieg, R. D.; "HONDO II A Finite Element Computer Program for the Large Deformation Dynamics Response of Axisymmetric Solids," SAND78-0422 (Albuquerque, New Mexico: Sandia National Laboratories, October 1978).

3. Hallquist, J. O.; "User's Manual for DYNA2D--An Explicit Two-Dimensional Hydrodynamic Finite Element Code with Interactive Re-zoning," UCID-18756 (Livermore, California: Lawrence Livermore Laboratory, February 1982).

4. Hallquist, J. O.; "User's Manual for DYNA3D and DYNAP: Nonlinear Dynamic Analysis of Solids in Three Dimensions," UCID-19156 (Livermore, California: Lawrence Livermore Laboratory, July 1981).

TABLE 1

Young's Modulus (E)	18000 psi
Poisson's Ratio (ν)	0.125
Yield Strength (σ_o)	1000 psi
Tangent Modulus (E_t)	1600 psi
Hardening Parameter ( )	0.0

TABLE II

Shear Modulus (G)	8000 psi
Bulk Unloading Modulus (K_o)	6000 psi
Yield Function Constants	
a_o	333333
a_1	0
a_2	0
Pressure Cutoff (F_p)	-2700 psi
Volumetric Strain-Pressure Pairs	

Strain	Pressure
0	0.
-0.0488	333.
-0.4055	600.
-0.5306	900.

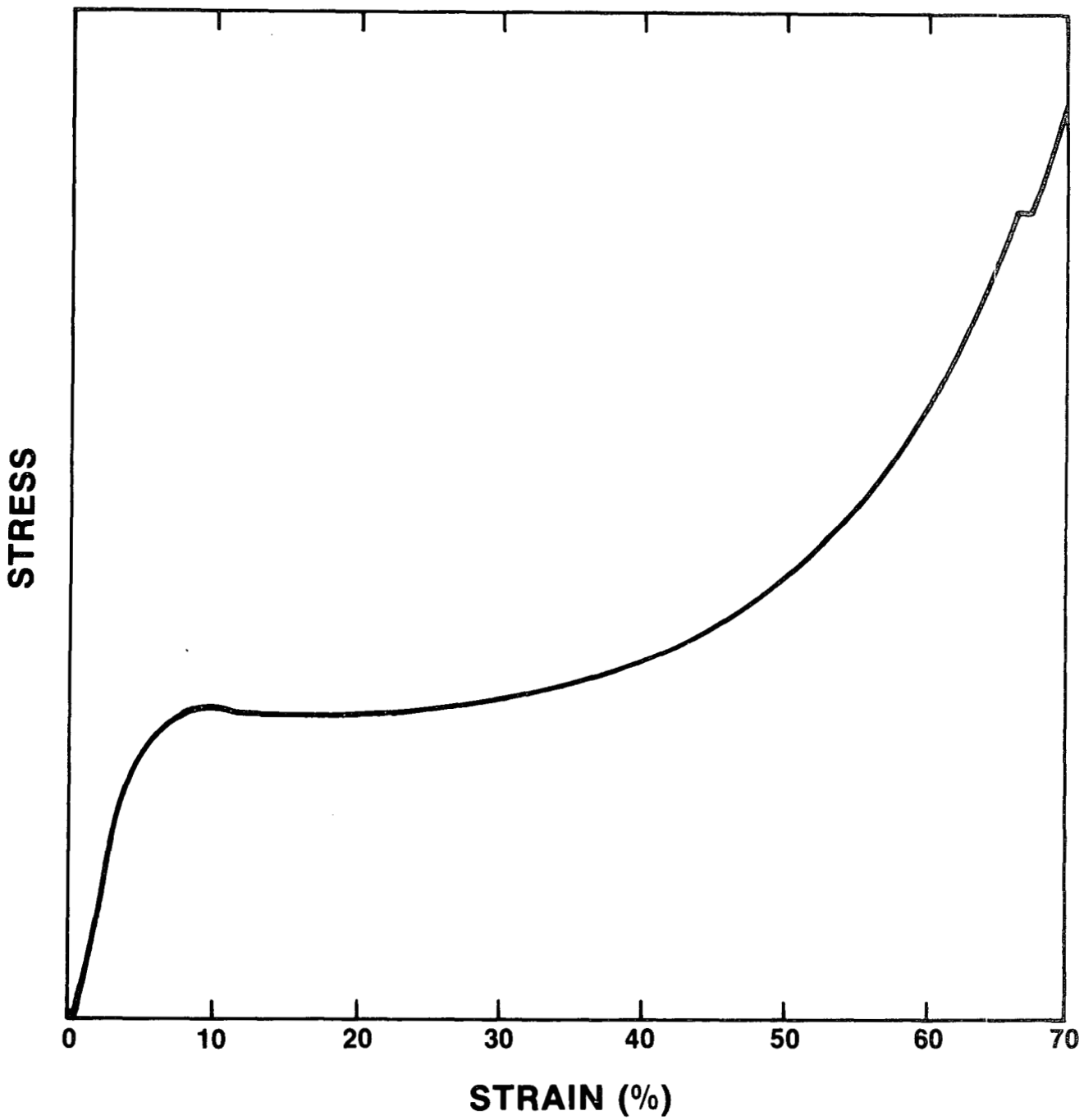

Figure 1. Typical Compression Test Results for Rigid Polyurethane Foam.

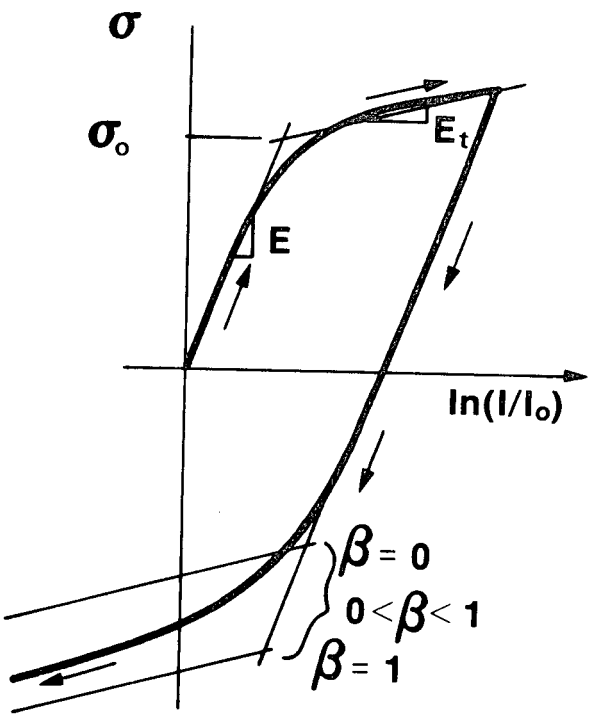

Figure 2. Graphical Description of the "Elastic-Plastic" Material Model.

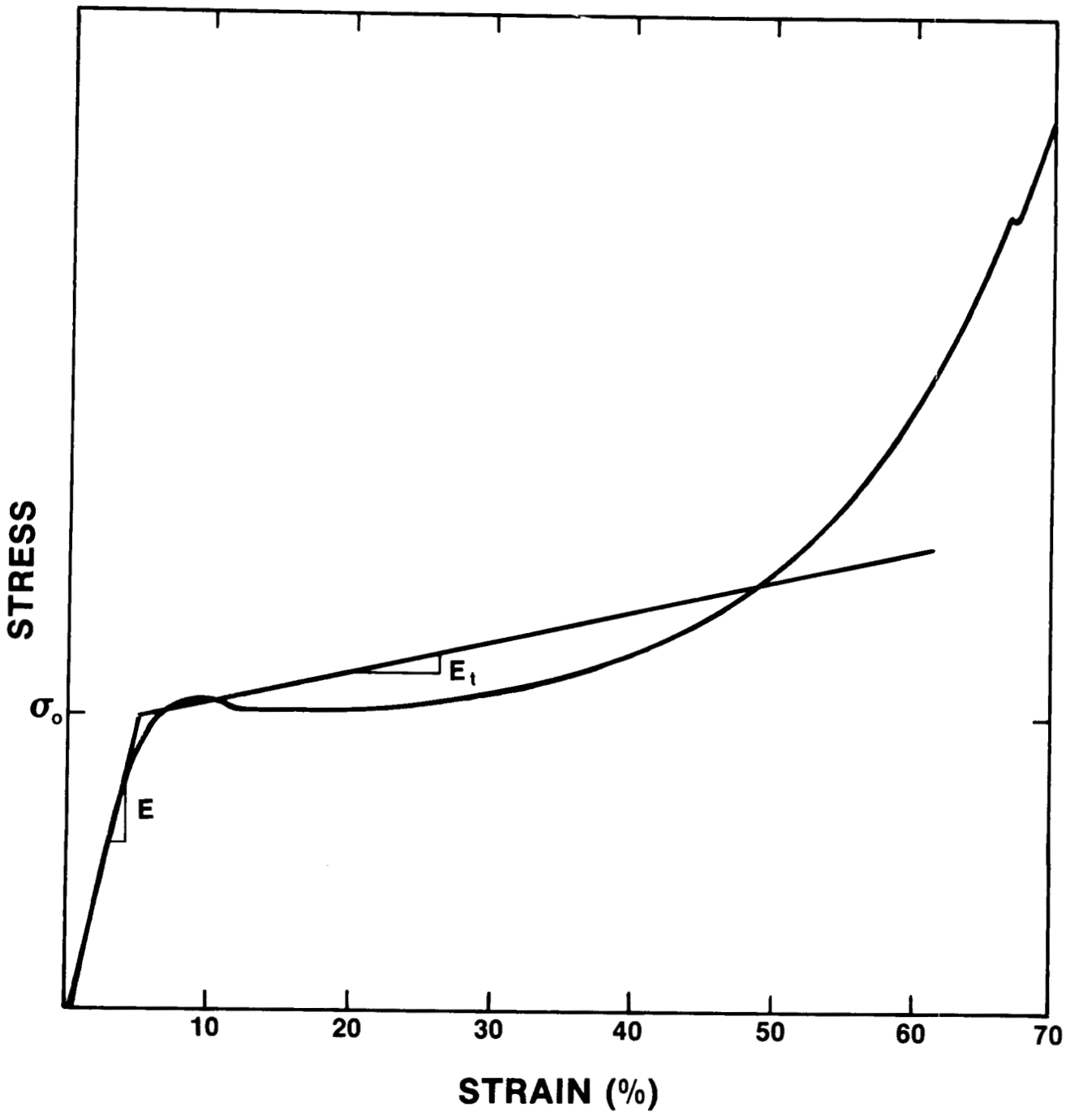

Figure 3. Estimation of the Rigid Foam Properties Using the "Elastic-Plastic" Material Model.

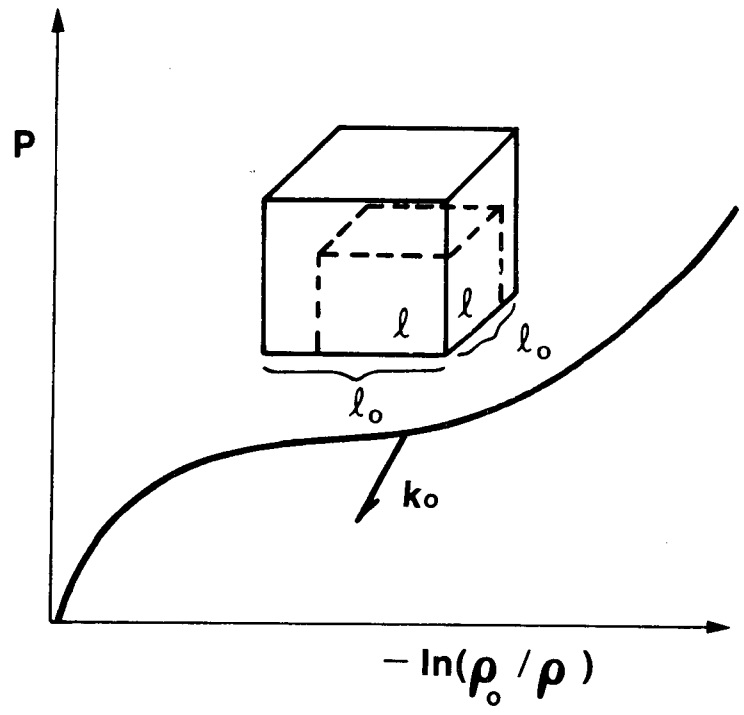

Figure 4. Graphical Description of the "Crushable Foam" Material Model

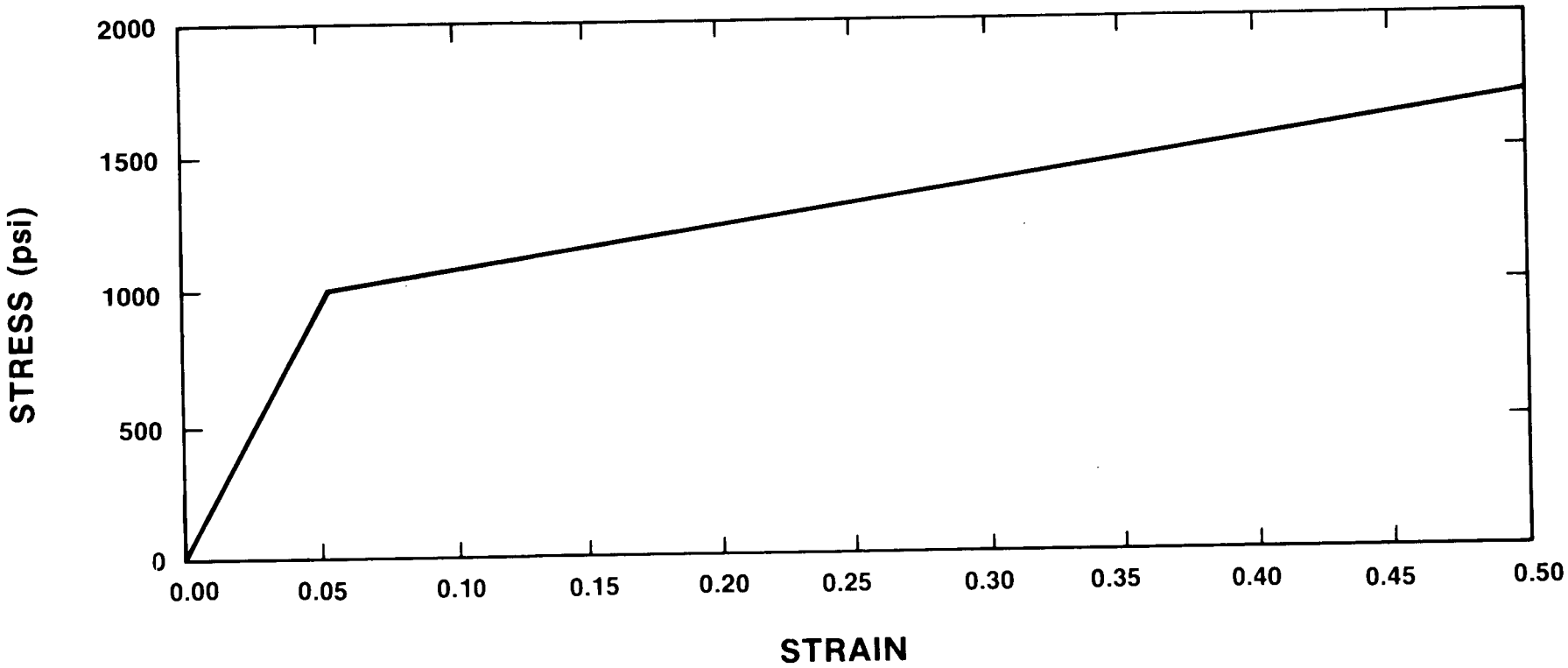

Figure 5. Stress-Strain Curve for 1000 PSI Foam Used as Input to the "Elastic-Plastic" Material Model.

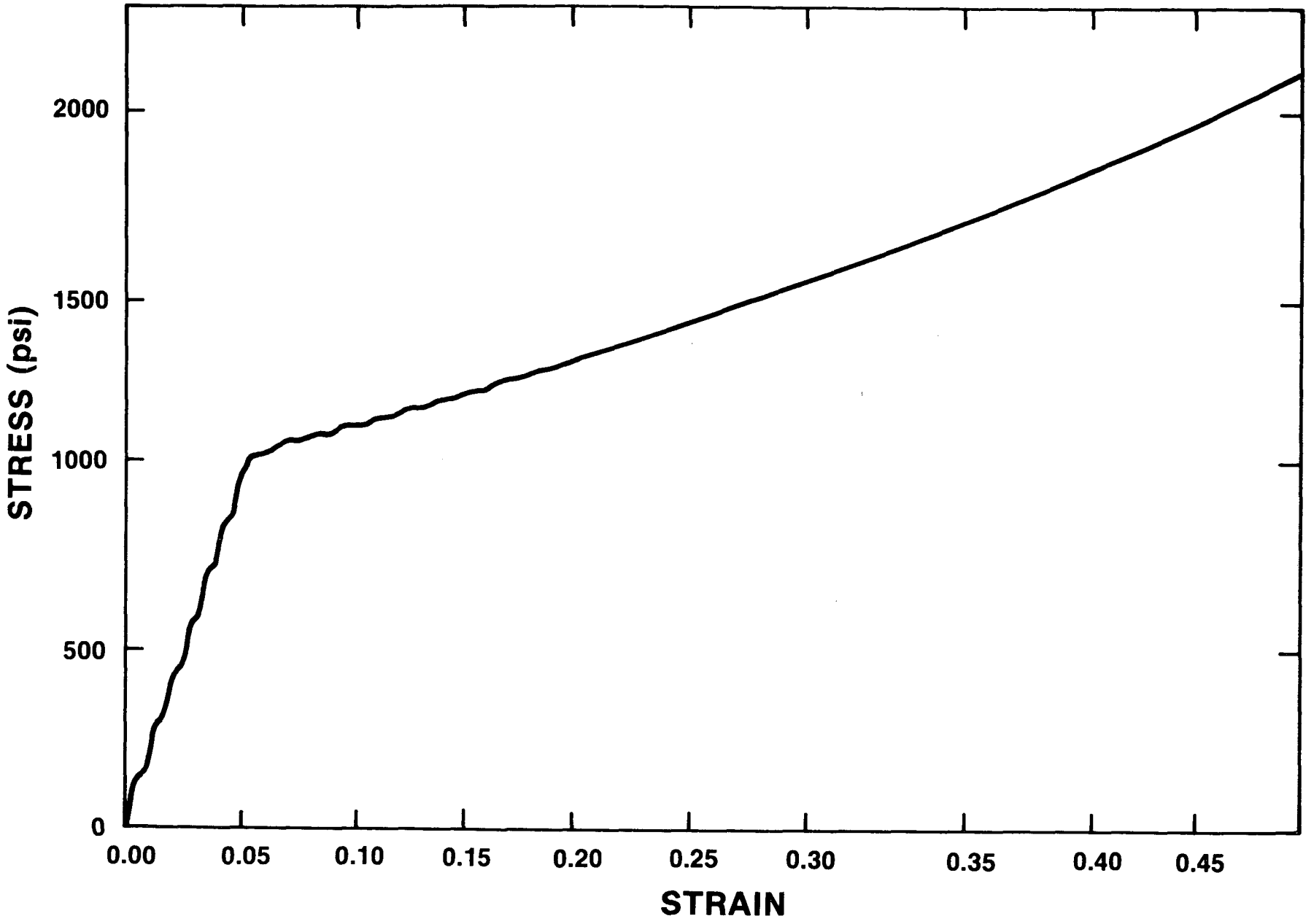

Figure 6. Unconstrained Cylinder, "Elastic-Plastic" Material Model Stress-Strain Curve

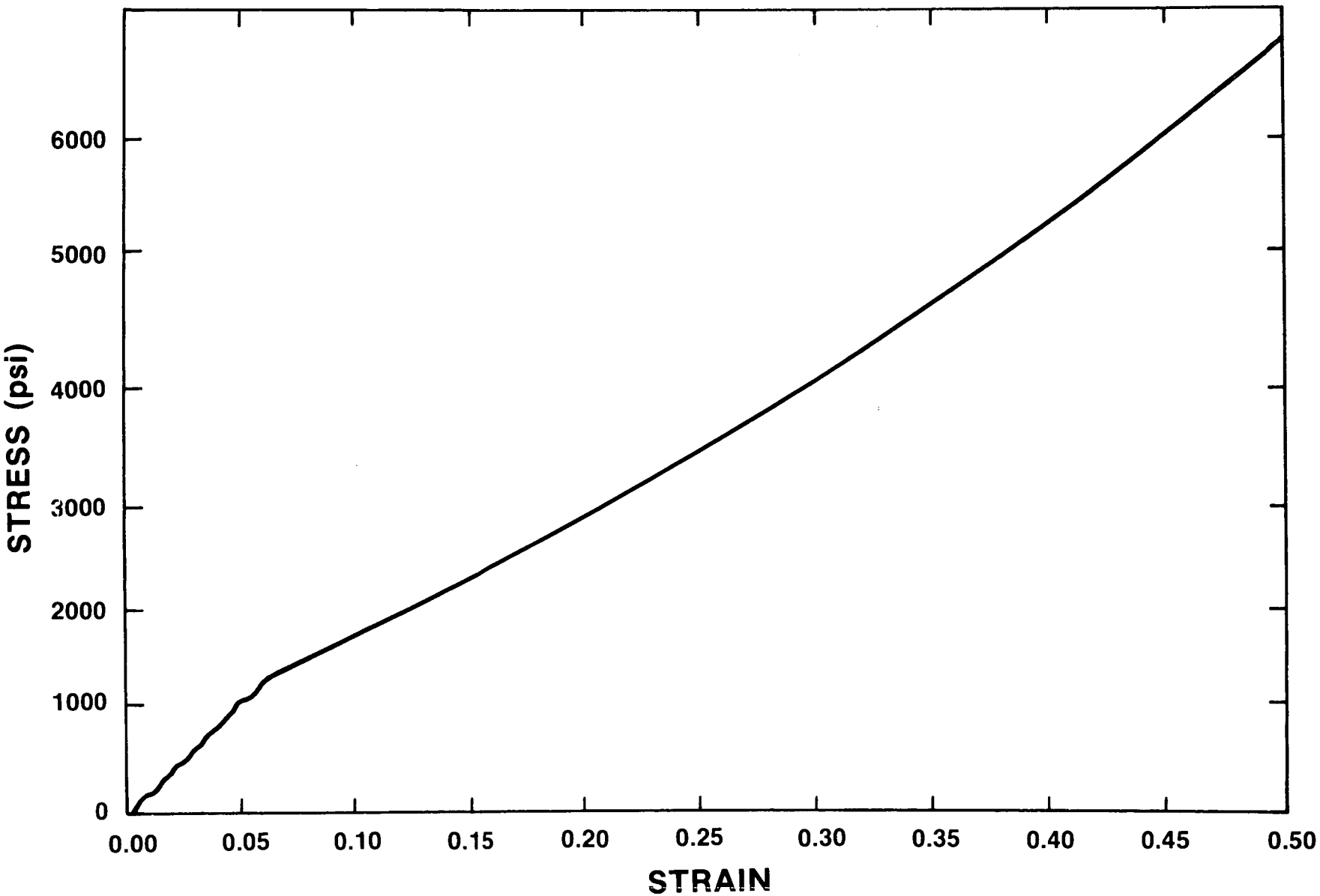

Figure 7. Laterally Constrained Cylinder,
"Elastic-Plastic" Material Model Stress-Strain Curve

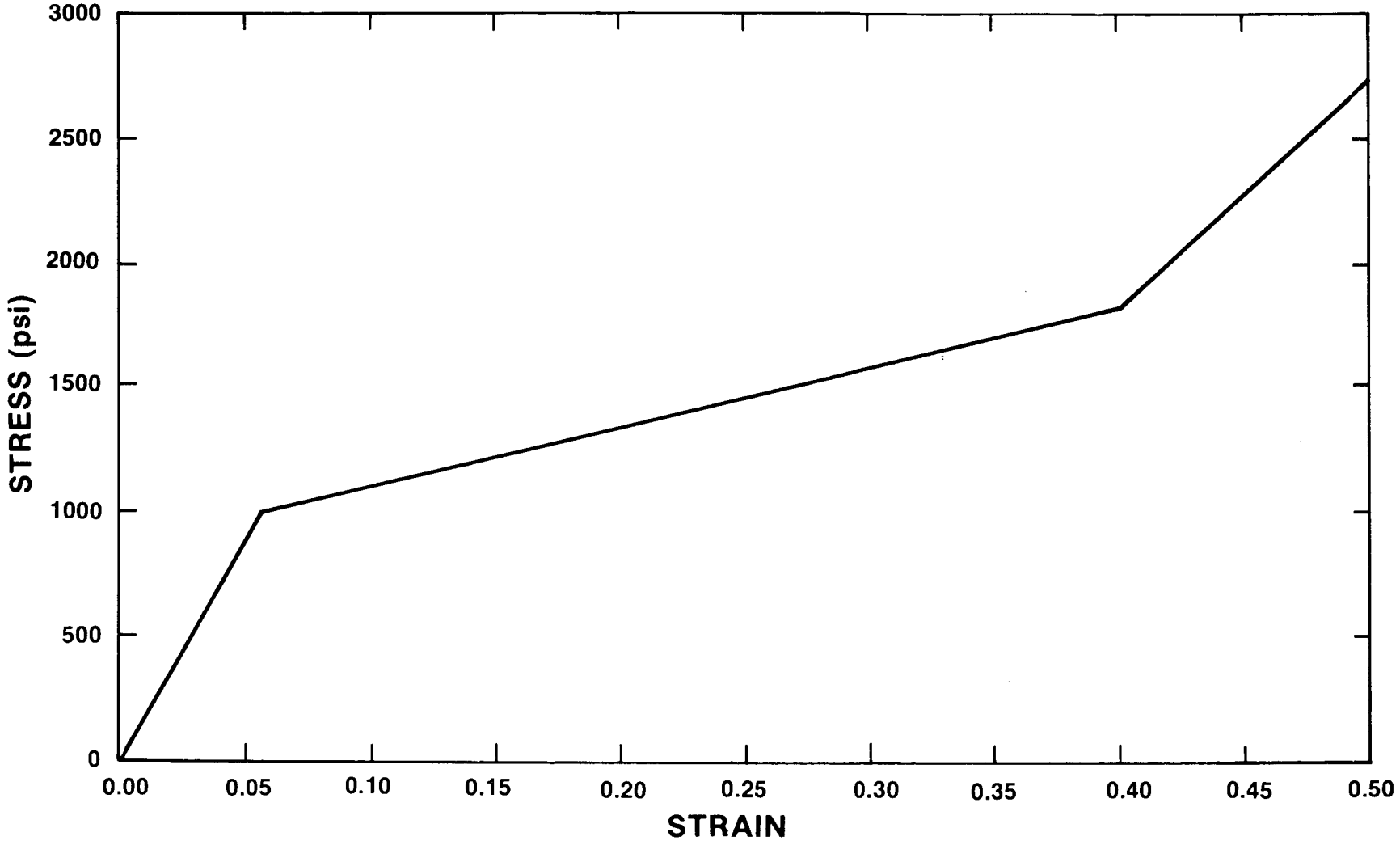

Figure 8. Stress-Strain Curve for 1000 PSI Foam Used as Input to the Crushable Foam Material Model

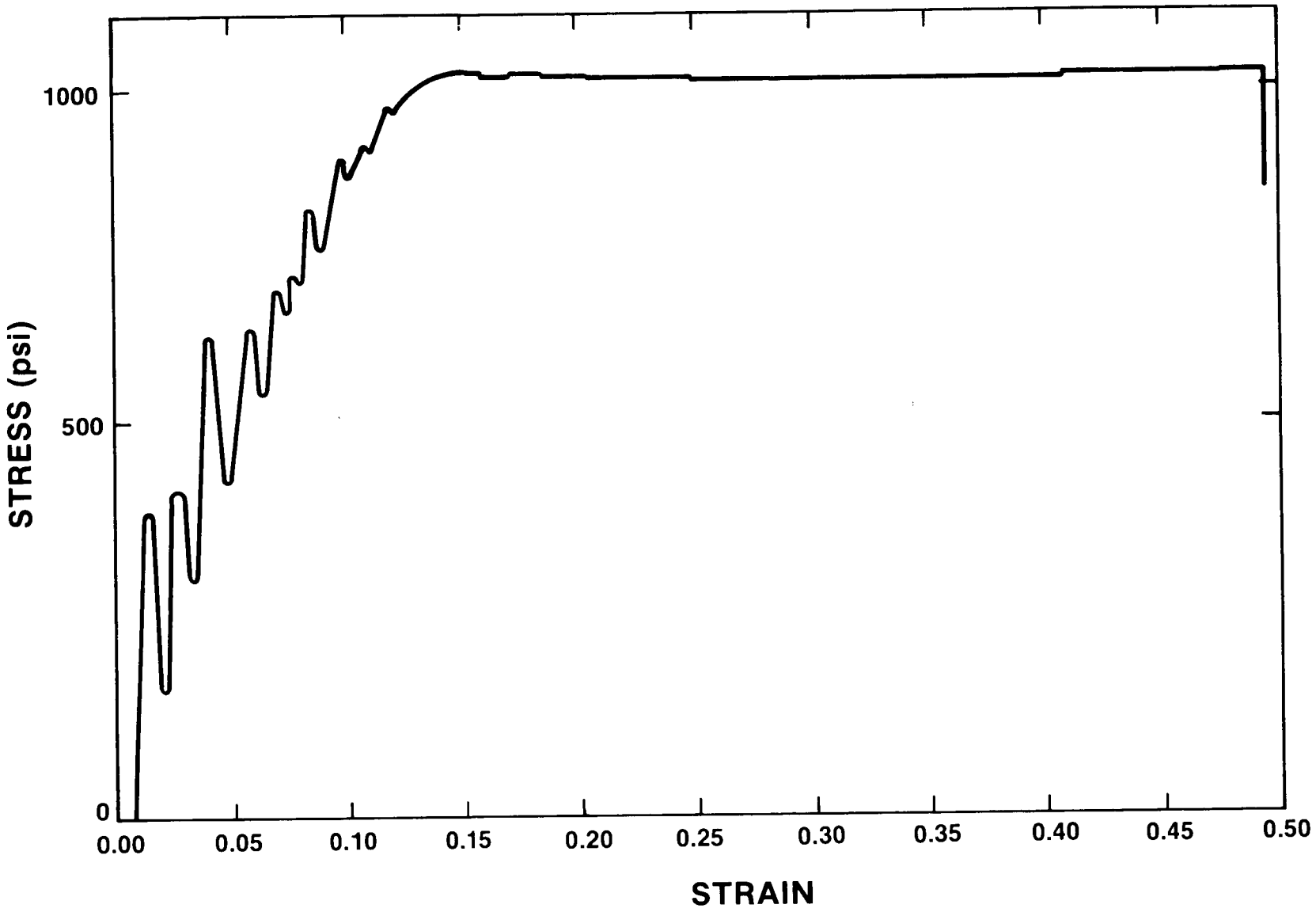

Figure 9. Unconstrained Cylinder, "Crushable Foam" Material Model Stress-Strain Curve

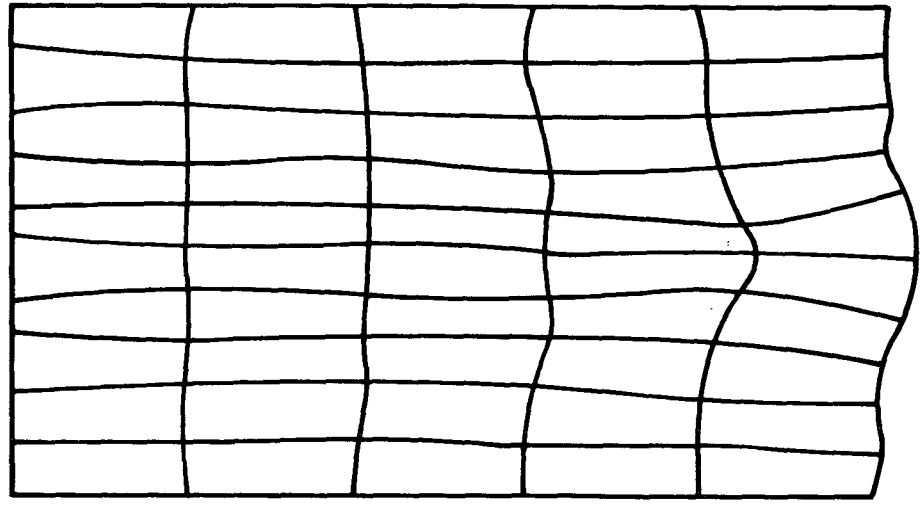

Figure 10. Deformed Shape At Maximum Strain for Unconstrained Cylinder Crushable Foam Analysis.

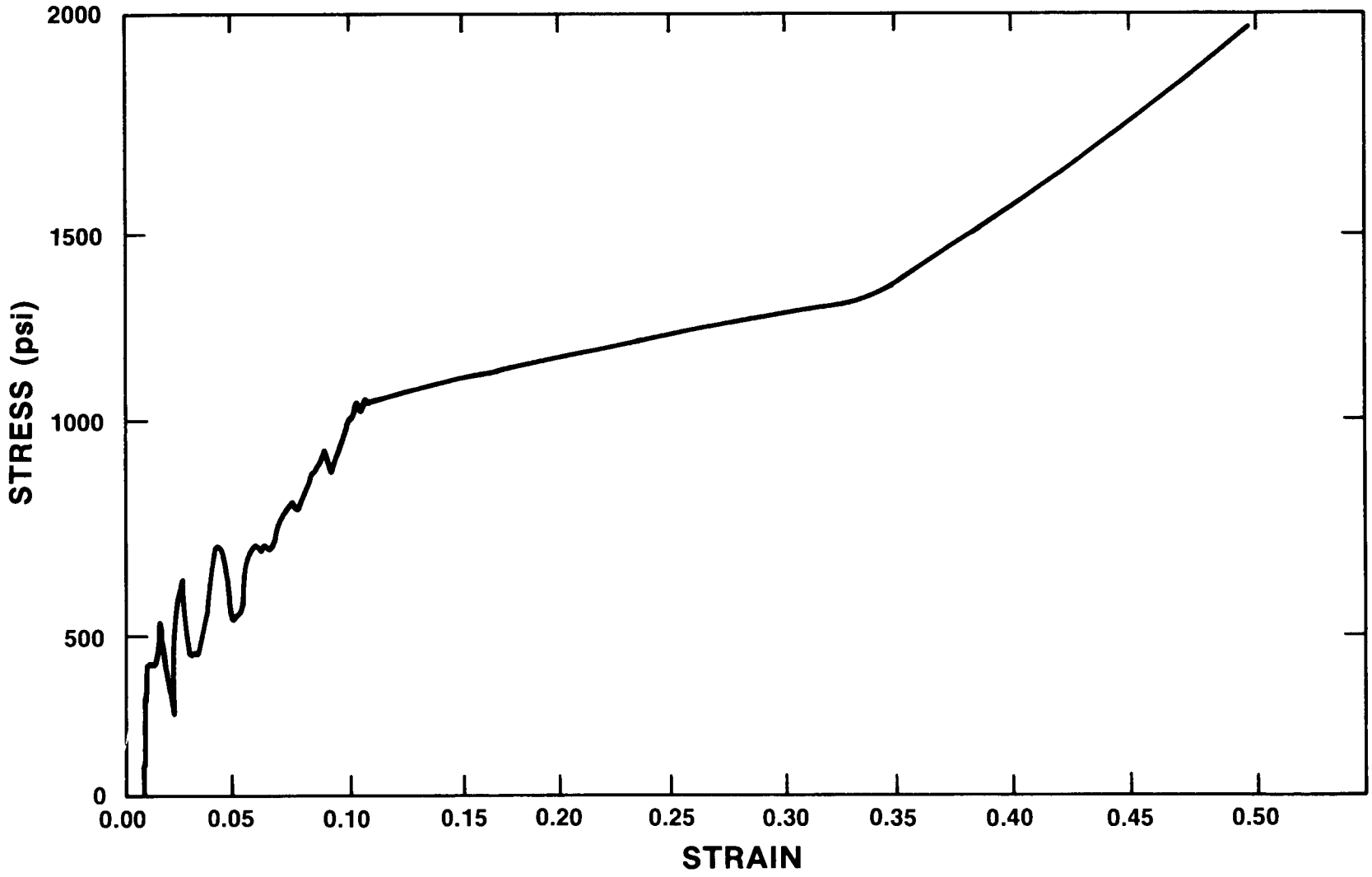

Figure 11. Laterally Constrained Cylinder, "Crushable Foam" Material Stress-Strain Curve

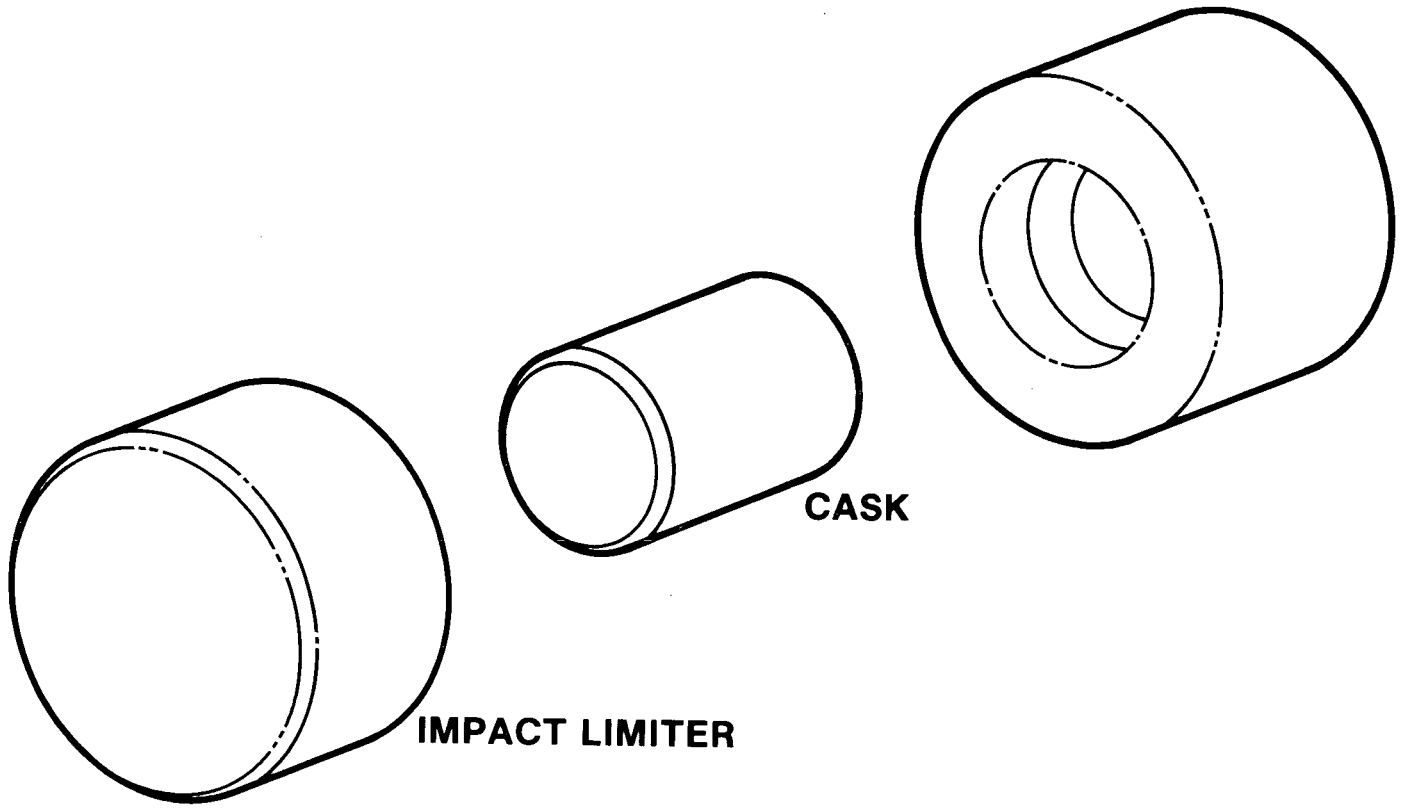

Figure 12. Original Half Scale Impact Limiter Test Configuration.

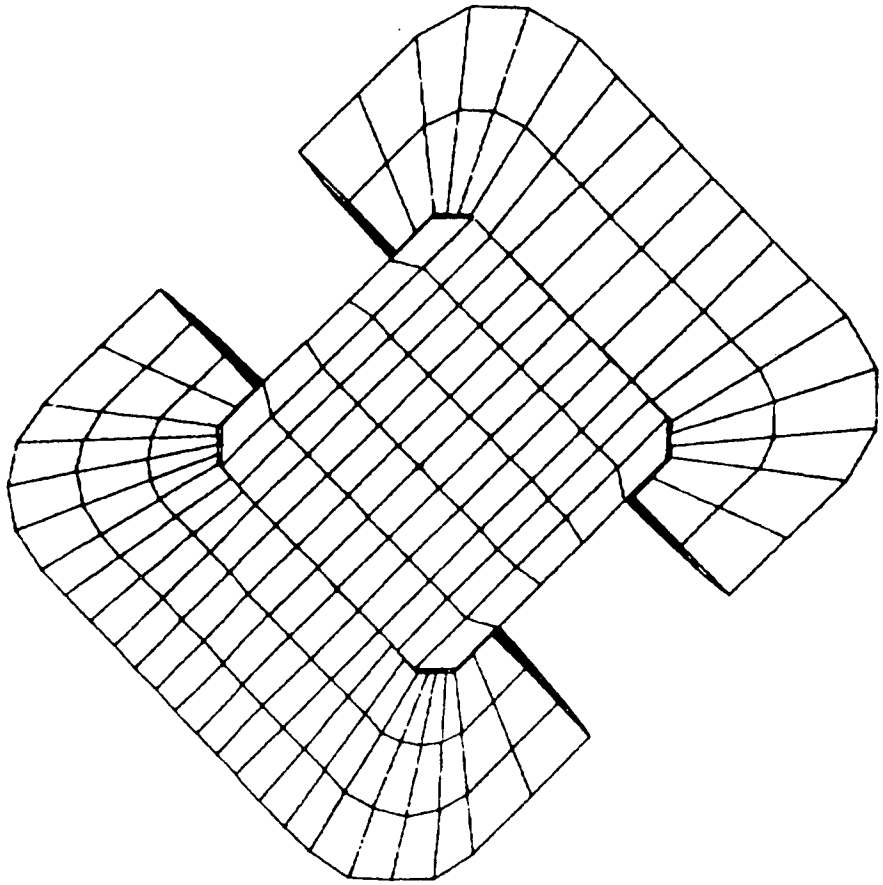

Figure 13. Corner Drop Hidden Line Plot of
Finite Element Mesh

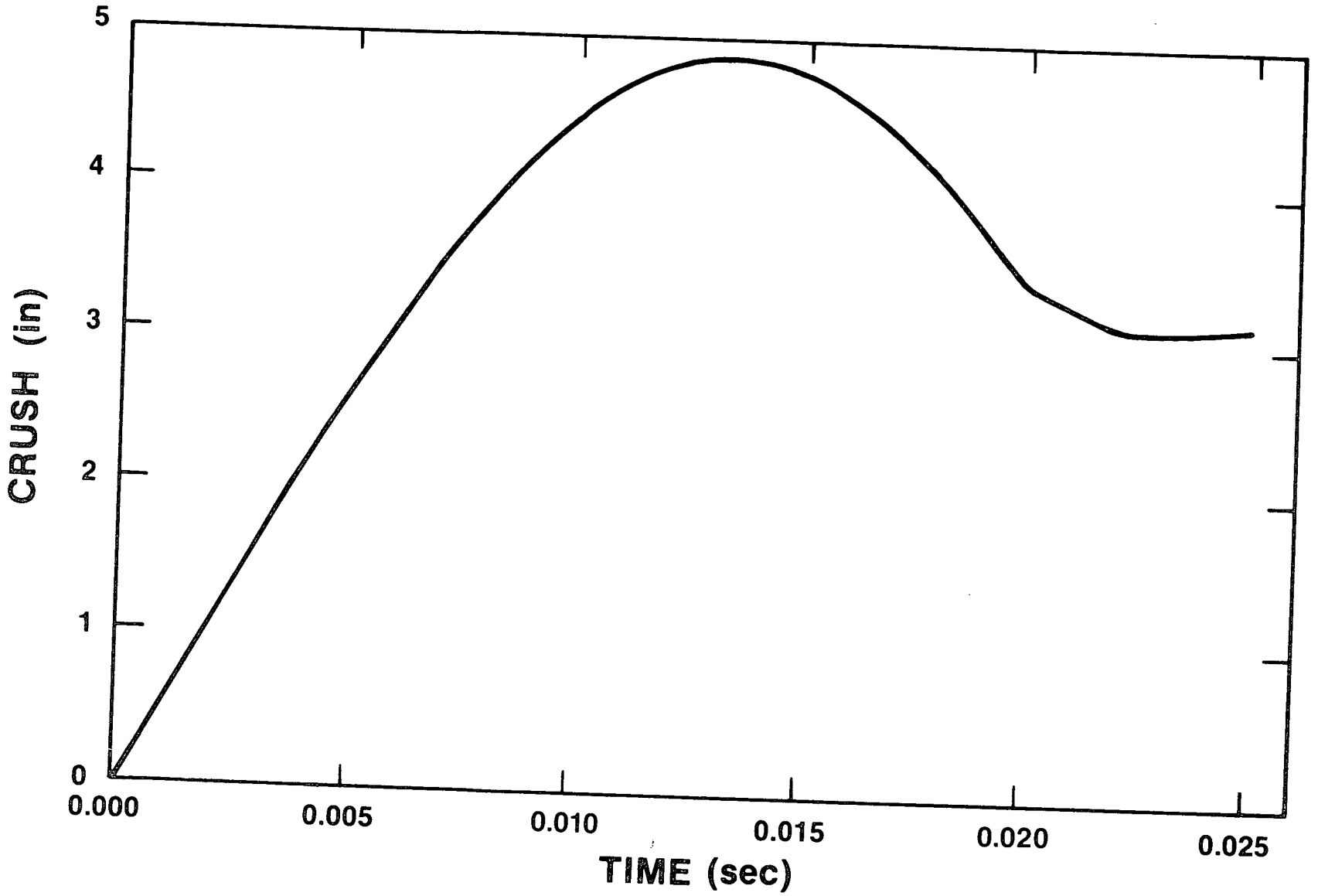

Figure 14. Corner Drop Impact Limiter Crush

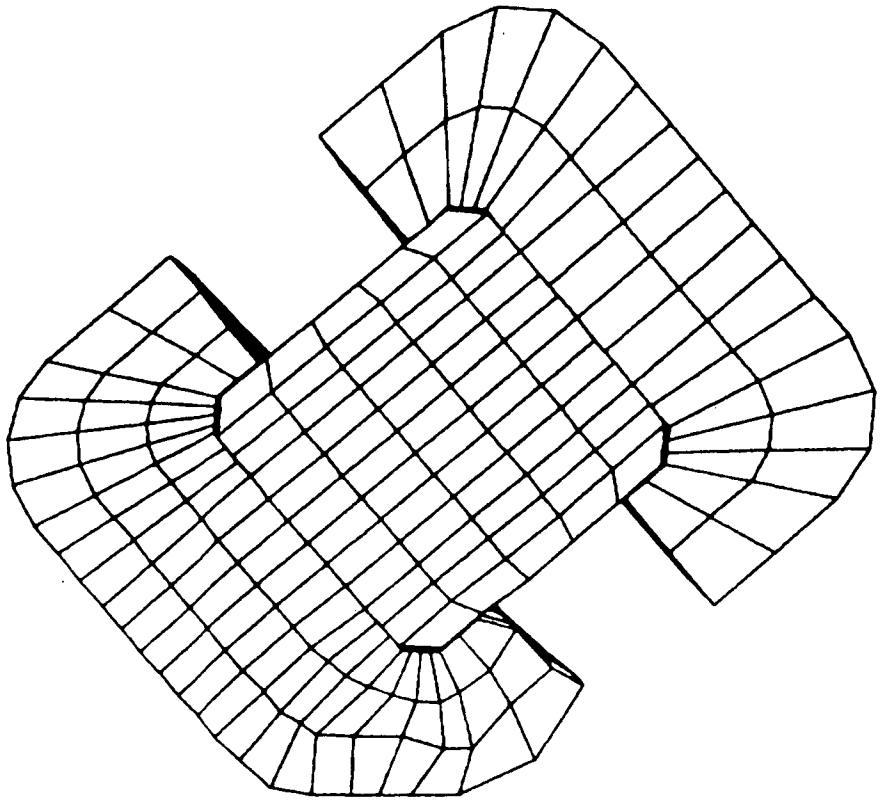

Figure 15. Corner Drop Deformed Shape at Maximum Crush (T = 0.013 Sec.)

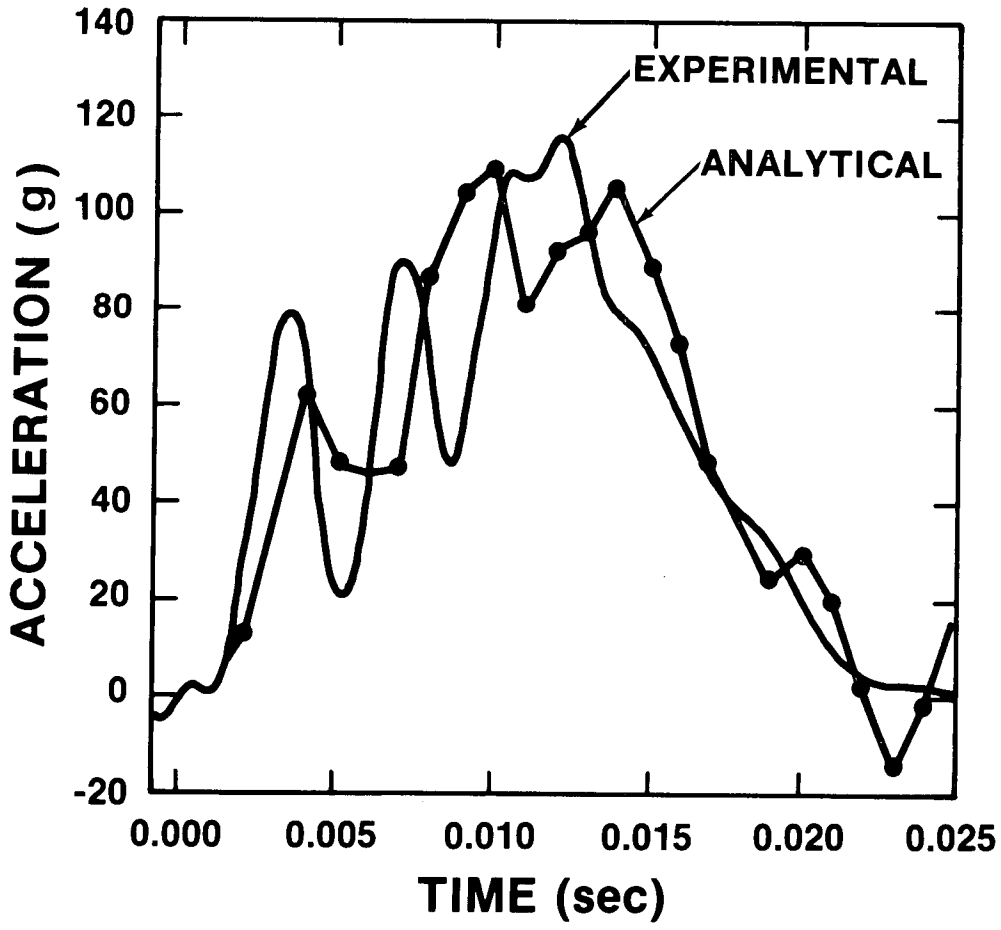

Figure 16. Corner Drop Experimental and Analytical Accelerations Parallel to Cask Axis.

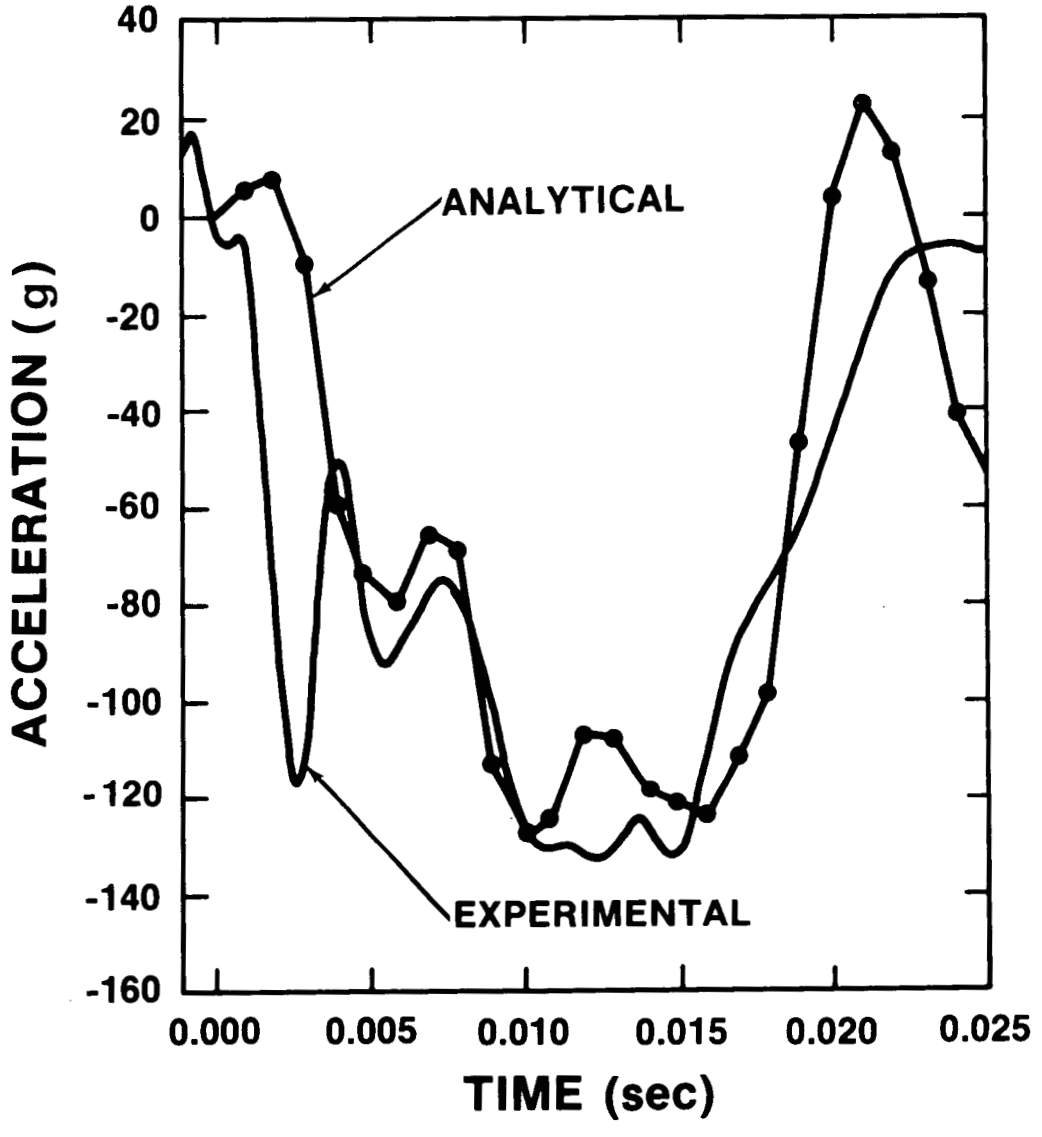

Figure 17. Corner Drop Experimental and Analytical Acceleration Transverse to Cask Axis.

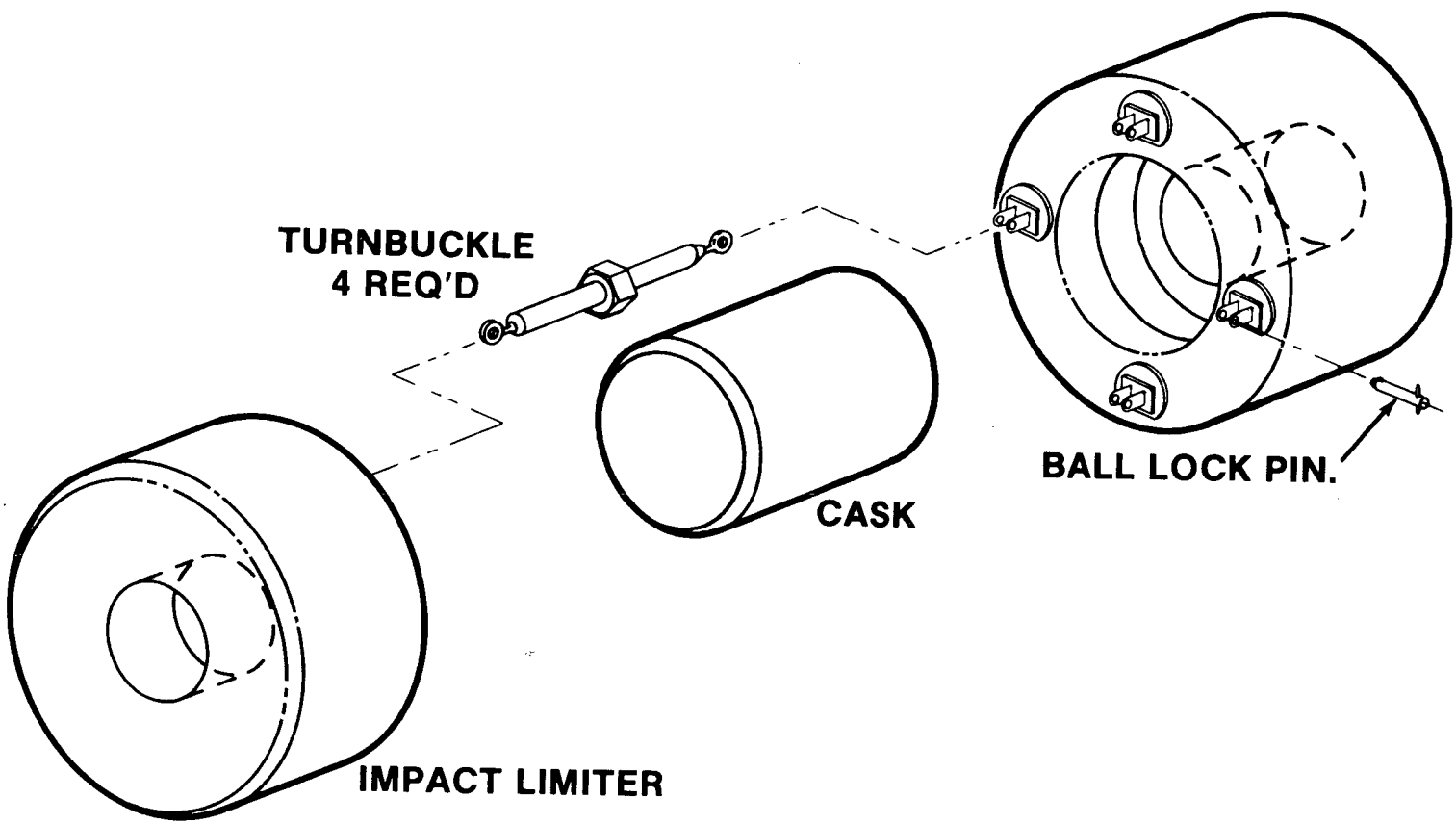

Figure 18. Modified Half Scale Impact Limiter Test Configuration

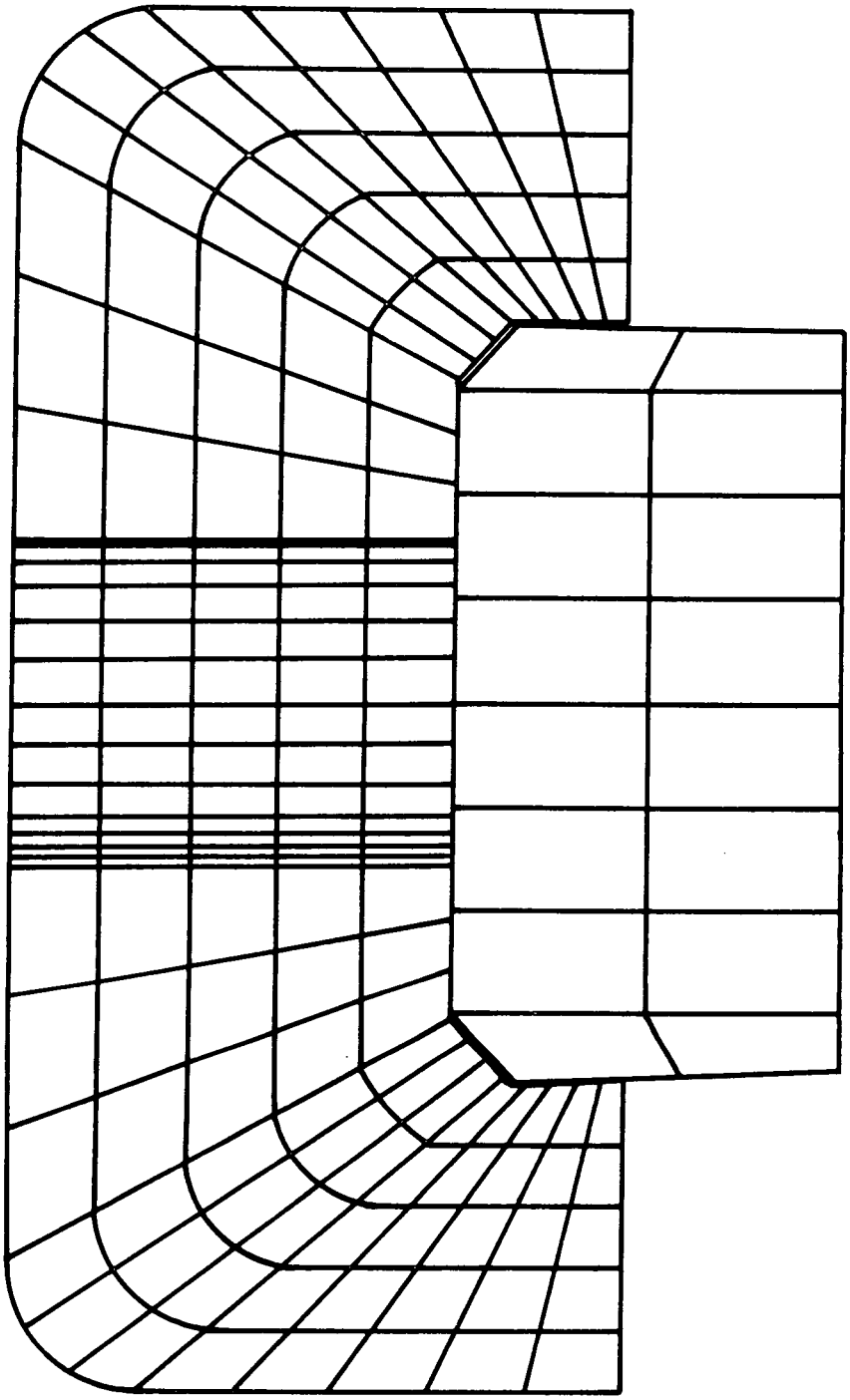

Figure 19. Side Drop 1000 PSI Hidden Line Plot of Finite Element Mesh

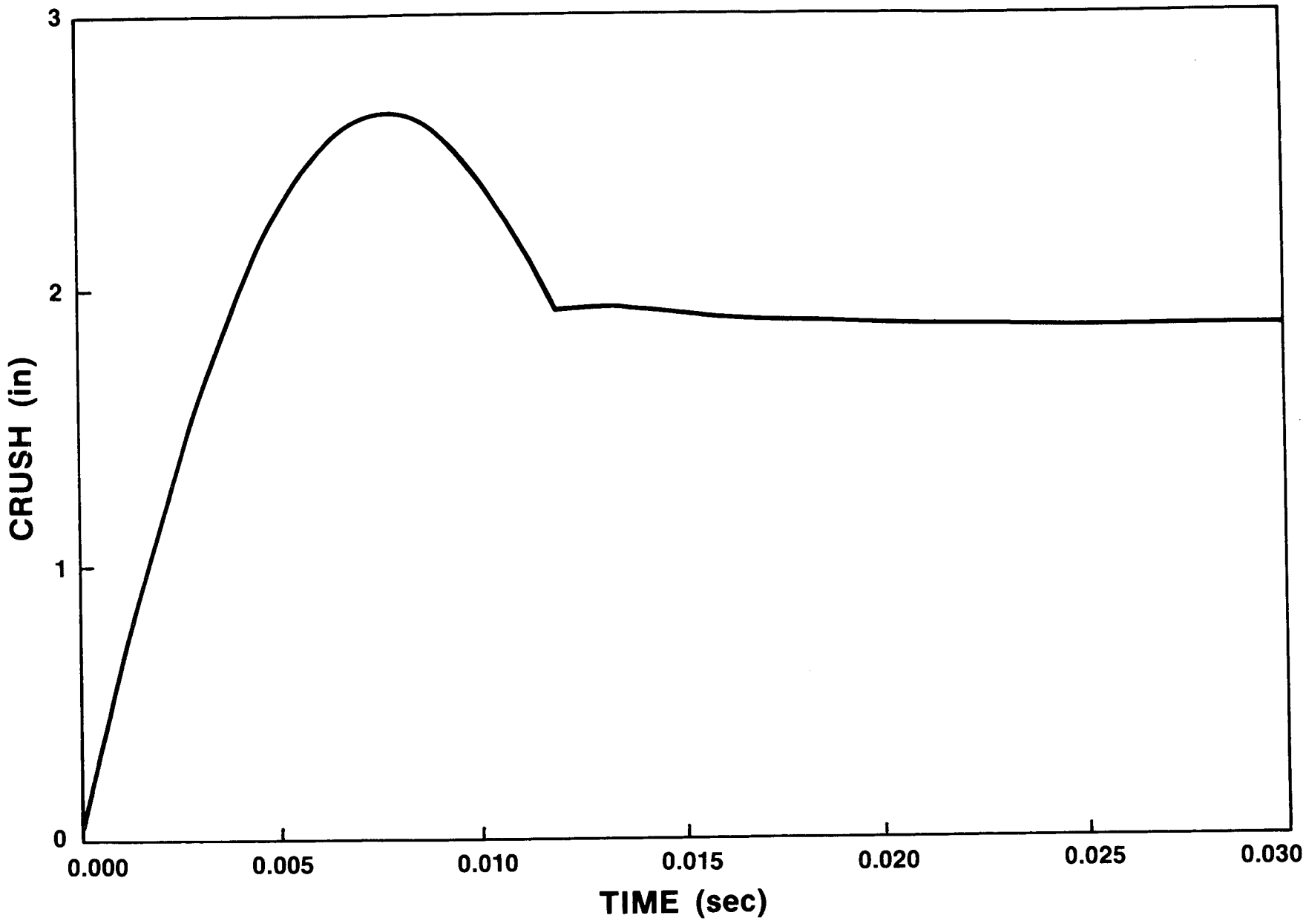

Figure 20. Side Drop 1000 PSI Foam Impact Limiter Crush

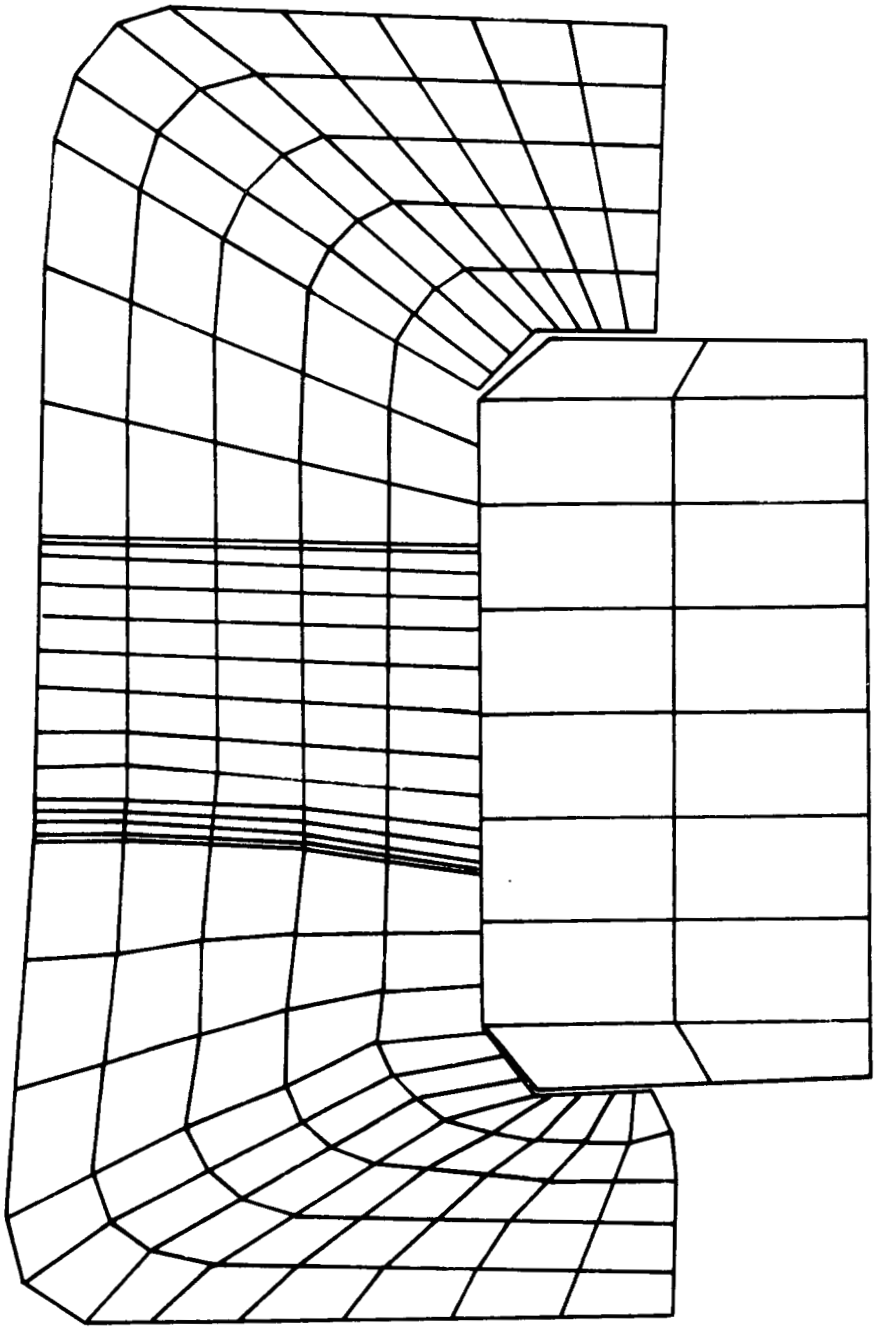

Figure 21. Side Drop 1000 PSI Foam Deformed Shape at Maximum Crush (T = 0.008 Sec)

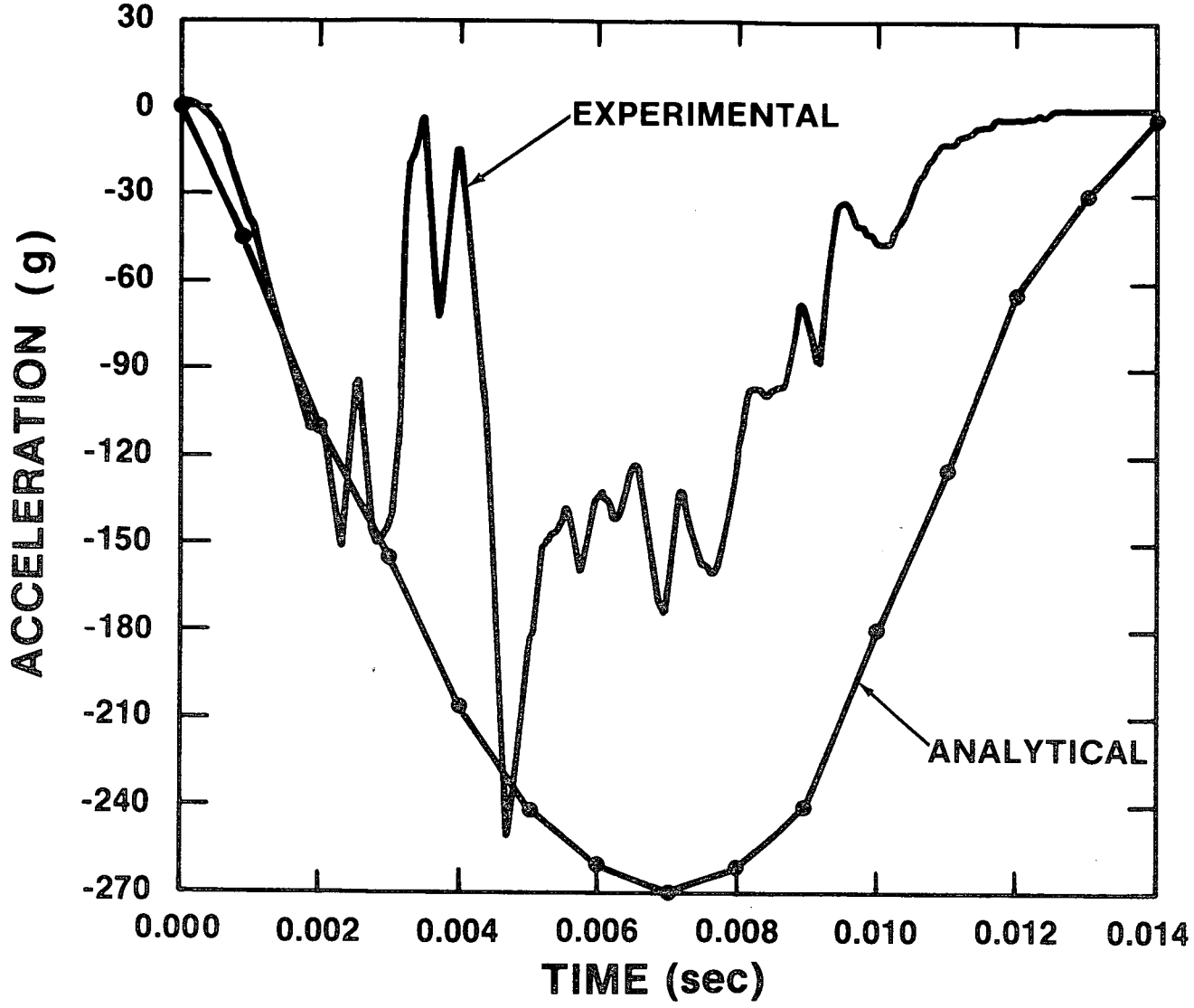

Figure 22. Side Drop 1000 PSI Foam Experimental and Analytical Acceleration

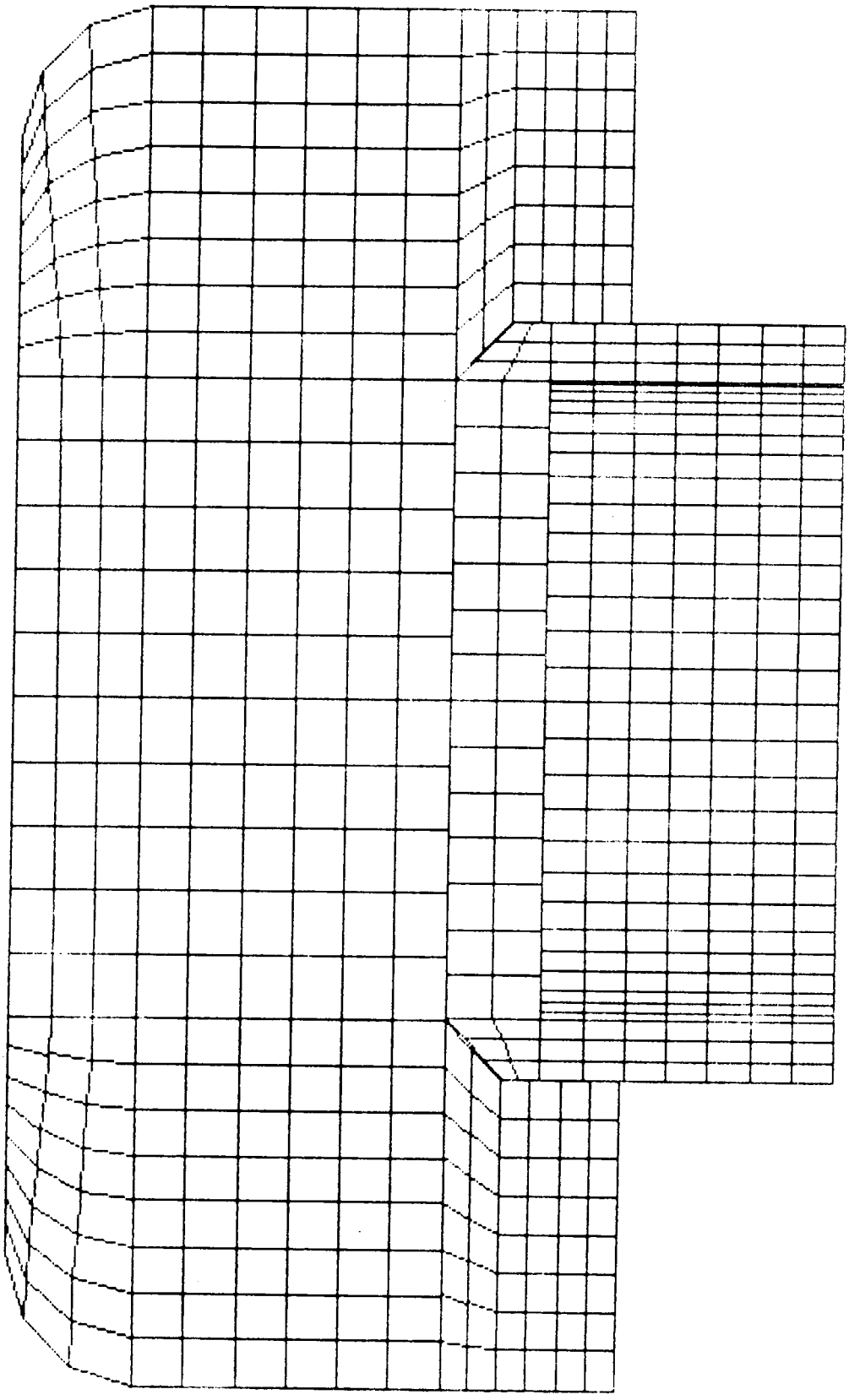

Figure 23. Side Drop 360 PSI Foam Hidden Line Plot of Finite Element Mesh

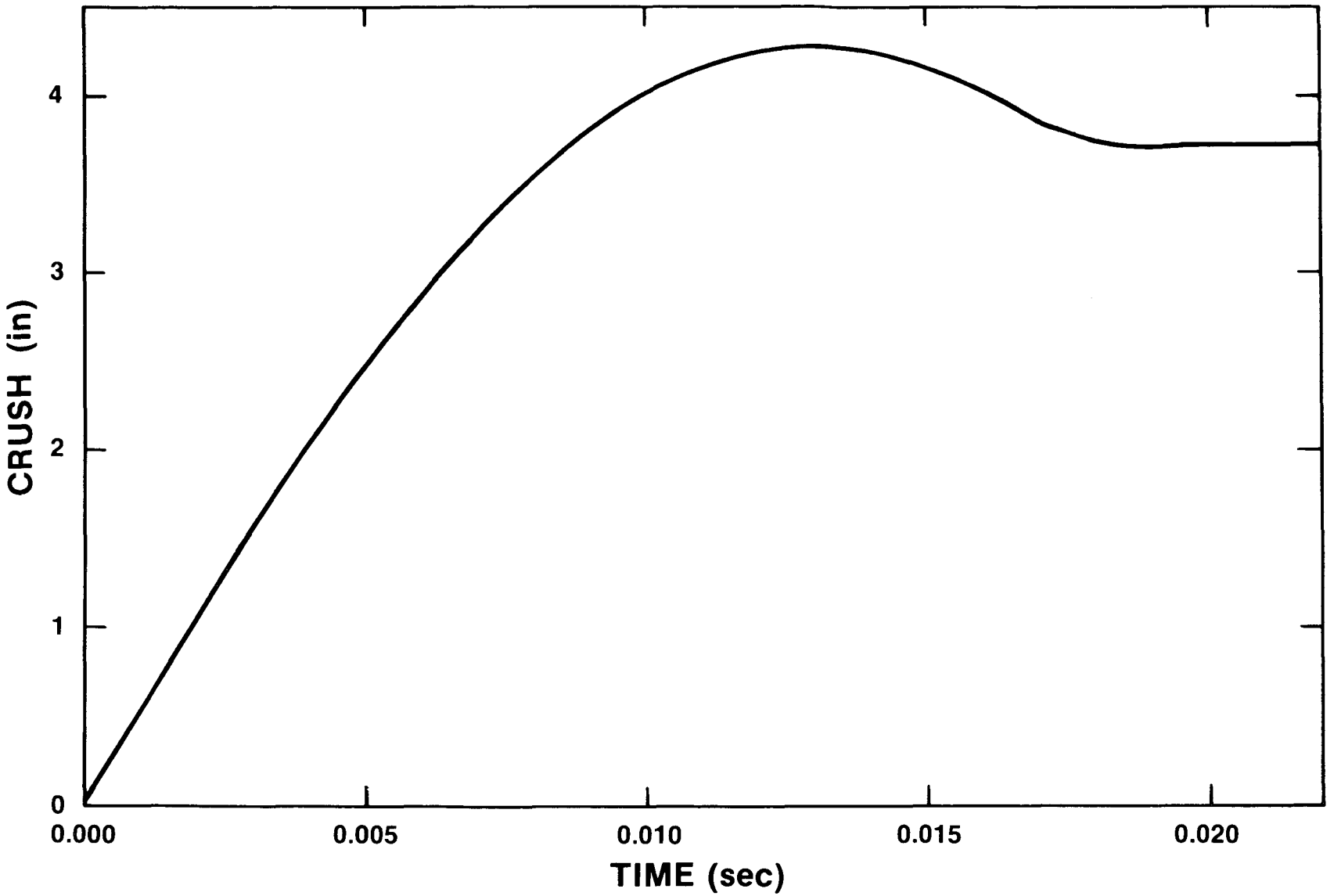

Figure 24. Side Drop 360 PSI Foam Impact Limiter Crush

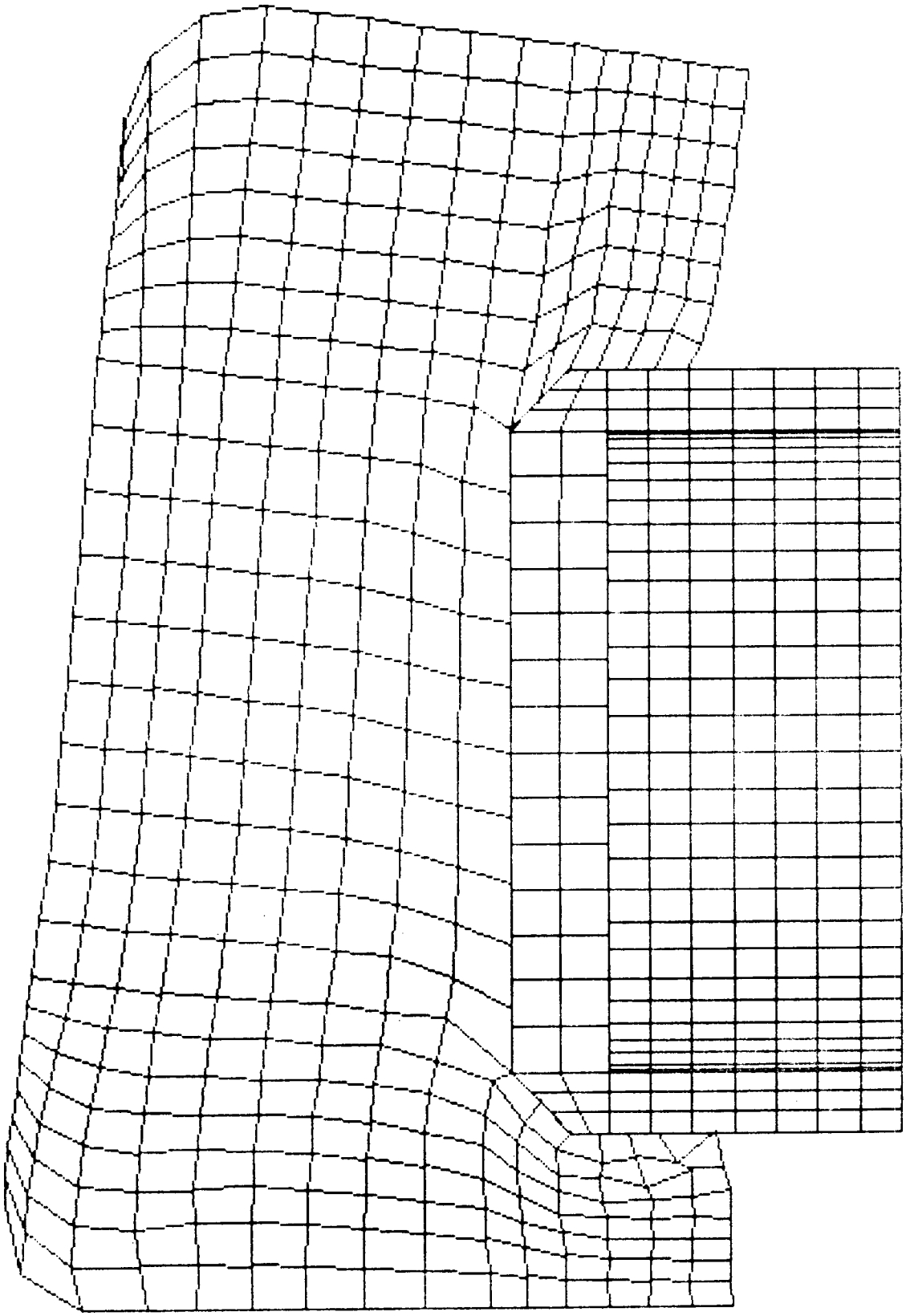

Figure 25. Side Drop 360 PSI Foam Deformed Shape at Maximum Crush (T = 0.013 Sec)

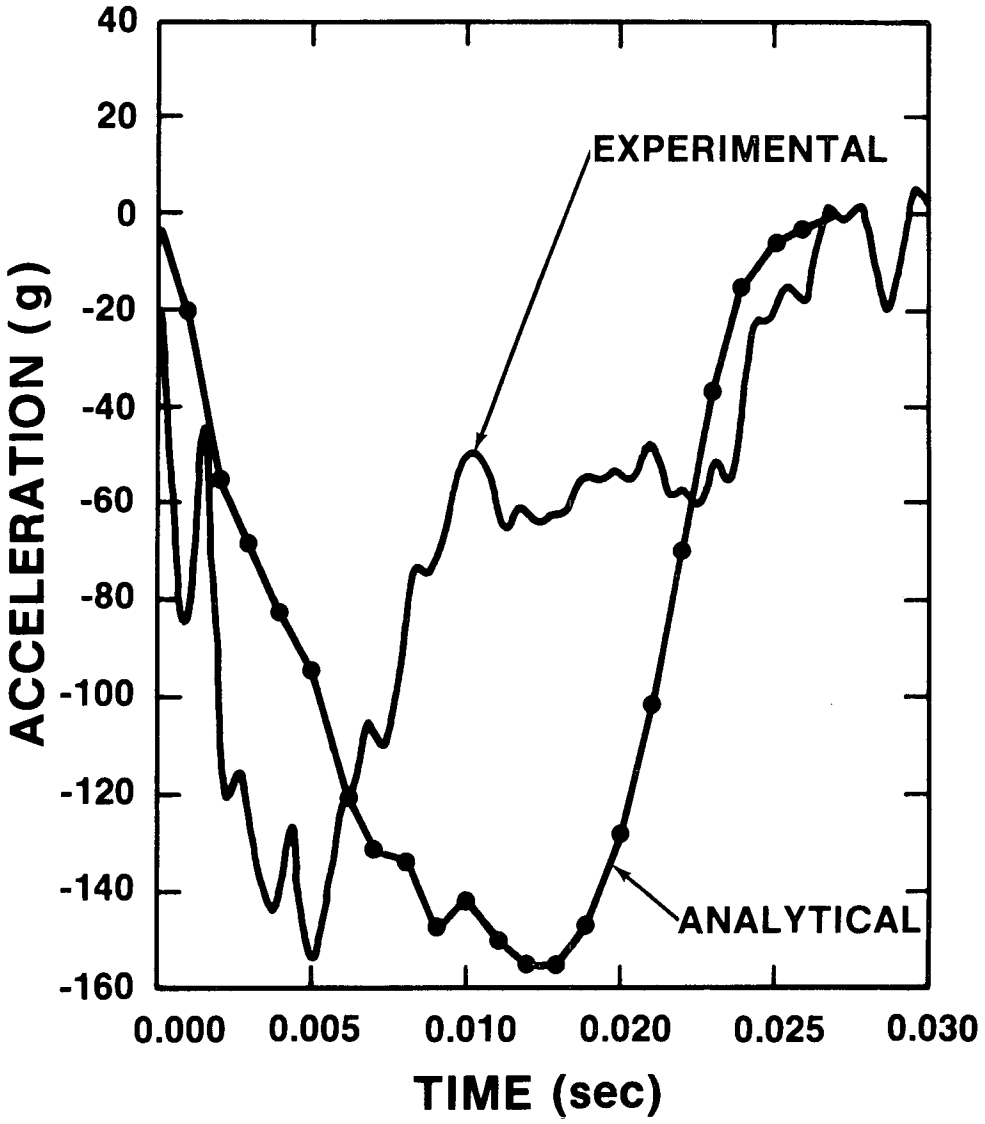

Figure 26. Side Drop 360 PSI Foam Experimental and Analytical Acceleration

DISTRIBUTION:

U. S. Department of Energy
Technical Information Center (100)
Oak Ridge, TN 37830
Attn: DOE/TIC-4500-R67 UC 71

U. S. Department of Energy
Routing DP 123
Washington, DC 20545
Attn: T. D. Anderson
J. Jicha
F. P. Falci

U. S. Department of Energy
Albuquerque Operations Office
Albuquerque, NM 87115
Attn: J. McGough
K. Golliher
E. C. Hardin
C. Anderson

1510 J. W. Nunziato
1520 D. J. McCloskey
1521 R. D. Krieg
1521 K. W. Gwinn
1521 M. K. Neilsen
1521 G. W. Wellman (15)
1530 L. W. Davison
1540 W. C. Luth
3141-1 C. M. Ostrander (5)
3151 W. L. Garner, For: (Unlimited Release for DOE/TIC) (3)
3154-3 C. H. Dalin, For: (Unlimited Release for DOE/TIC (28)
6000 E. H. Beckner
6300 R. W. Lynch
6320 J. F. Ney
Attn: TTC Master File
6320 TTC Library (25)
6321 R. E. Luna
6322 W. E. Wowak
6323 G. C. Allen, Jr.
6323 H. R. Yoshimura (5)
6323 A. Gonzales
6324 B. D. Zak
8024 M. A. Pound